


























IceCat-1: the IceCube Event Catalog of Alert Tracks

R. ABBASI ¹⁷, M. ACKERMANN ⁶⁴, J. ADAMS¹⁸, S. K. AGARWALLA ⁴¹, * J. A. AGUILAR ¹², M. AHLERS ²²,
J.M. ALAMEDDINE ²³, N. M. AMIN⁴⁵, K. ANDEEN⁴³, G. ANTON ²⁶, C. ARGÜELLES ¹⁴, Y. ASHIDA⁴¹,
S. ATHANASIADOU⁶⁴, S. N. AXANI ⁴⁵, X. BAI ⁵¹, A. BALAGOPAL V. ⁴¹, M. BARICEVIC⁴¹, S. W. BARWICK ³⁰,
V. BASU ⁴¹, R. BAY⁸, J. J. BEATTY ^{20,21}, K.-H. BECKER⁶³, J. BECKER TJUS ¹¹, † J. BEISE ⁶², C. BELLENGHI ⁶⁵,
S. BENZVI ⁵³, D. BERLEY¹⁹, E. BERNARDINI ⁴⁹, D. Z. BESSON³⁶, G. BINDER^{8,9}, D. BINDIG⁶³, E. BLAUFUSS ¹⁹,
S. BLOT ⁶⁴, F. BONTEMPO³¹, J. Y. BOOK ¹⁴, C. BOSCOLO MENEGUOLO ⁴⁹, S. BÖSER ⁴², O. BOTNER ⁶²,
J. BÖTTCHER¹, E. BOURBEAU²², J. BRAUN⁴¹, B. BRINSON⁶, J. BROSTEAN-KAISER⁶⁴, R. T. BURLEY², R. S. BUSSE⁴⁴,
D. BUTTERFIELD⁴¹, M. A. CAMPANA ⁵⁰, K. CARLONI¹⁴, E. G. CARNIE-BRONCA², S. CHATTOPADHYAY⁴¹, * N. CHAU¹²,
C. CHEN ⁶, Z. CHEN⁵⁶, D. CHIRKIN ⁴¹, S. CHOI⁵⁷, B. A. CLARK ¹⁹, L. CLASSEN⁴⁴, A. COLEMAN ⁶², G. H. COLLIN¹⁵,
A. CONNOLLY^{20,21}, J. M. CONRAD ¹⁵, P. COPPIN ¹³, P. CORREA ¹³, S. COUNTRYMAN⁴⁷, D. F. COWEN^{60,61},
P. DAVE ⁶, C. DE CLERCQ ¹³, J. J. DELAUNAY ⁵⁹, D. DELGADO ¹⁴, H. DEMBINSKI ⁴⁵, S. DENG¹, K. DEOSKAR⁵⁵,
A. DESAI ⁴¹, P. DESIATI ⁴¹, K. D. DE VRIES ¹³, G. DE WASSEIGE ³⁸, T. DEYOUNG ²⁴, A. DIAZ ¹⁵,
J. C. DÍAZ-VÉLEZ ⁴¹, M. DITTMER⁴⁴, A. DOMI²⁶, H. DUJMOVIC ⁴¹, M. A. DUVERNOIS ⁴¹, T. EHRHARDT⁴²,
P. ELLER ⁶⁵, R. ENGEL^{31,32}, H. ERPENBECK⁴¹, J. EVANS¹⁹, P. A. EVENSON⁴⁵, K. L. FAN¹⁹, K. FANG⁴¹, K. FARRAG¹⁶,
A. R. FAZELY ⁷, A. FEDYNITCH ⁵⁸, N. FEIGL¹⁰, S. FIEDLSCHUSTER²⁶, C. FINLEY ⁵⁵, L. FISCHER⁶⁴, D. FOX ⁶⁰,
A. FRANCKOWIAK ¹¹, E. FRIEDMAN¹⁹, A. FRITZ⁴², P. FÜRST¹, T. K. GAISSER ⁴⁵, J. GALLAGHER⁴⁰, E. GANSTER ¹,
A. GARCIA ¹⁴, L. GERHARDT⁹, A. GHADIMI ⁵⁹, C. GLASER⁶², T. GLAUCH ⁶⁵, T. GLÜSENKAMP ^{26,62}, N. GOEHLKE³²,
J. G. GONZALEZ⁴⁵, S. GOSWAMI⁵⁹, D. GRANT²⁴, S. J. GRAY ¹⁹, S. GRIFFIN⁴¹, S. GRISWOLD ⁵³, C. GÜNTHER¹,
P. GUTJAHR ²³, C. HAACK⁶⁵, A. HALLGREN ⁶², R. HALLIDAY²⁴, L. HALVE ¹, F. HALZEN ⁴¹, H. HAMDAOUI ⁵⁶,
M. HA MINH⁶⁵, K. HANSON⁴¹, J. HARDIN¹⁵, A. A. HARNISCH²⁴, P. HATCH³³, A. HAUNGS ³¹, K. HELBING ⁶³,
J. HELLRUNG¹¹, F. HENNINGSEN ⁶⁵, L. HEUERMANN¹, N. HEYER⁶², S. HICKFORD⁶³, A. HIDVEGI⁵⁵, C. HILL ¹⁶,
G. C. HILL², K. D. HOFFMAN¹⁹, K. HOSHINA⁴¹, ‡ W. HOU ³¹, T. HUBER ³¹, K. HULTQVIST ⁵⁵, M. HÜNNEFELD ²³,
R. HUSSAIN⁴¹, K. HYMON²³, S. IN⁵⁷, A. ISHIHARA¹⁶, M. JACQUART⁴¹, O. JANIK¹, M. JANSSON⁵⁵, G. S. JAPARIDZE ⁵,
K. JAYAKUMAR⁴¹, * M. JEONG⁵⁷, M. JIN ¹⁴, B. J. P. JONES ⁴, D. KANG ³¹, W. KANG ⁵⁷, X. KANG⁵⁰,
A. KAPPES ⁴⁴, D. KAPPESSER⁴², L. KARDUM²³, T. KARG ⁶⁴, M. KARL ⁶⁵, A. KARLE ⁴¹, U. KATZ ²⁶,
M. KAUER ⁴¹, J. L. KELLEY ⁴¹, A. KHATEE ZATHUL ⁴¹, A. KHEIRANDISH ^{34,35}, J. KIRYLUK ⁵⁶, S. R. KLEIN ^{8,9},
A. KOCHOCKI ²⁴, R. KOIRALA ⁴⁵, H. KOLANOSKI ¹⁰, T. KONTRIMAS ⁶⁵, L. KÖPKE⁴², C. KOPPER ²⁴,
D. J. KOSKINEN ²², P. KOUNDAL ³¹, M. KOVACEVICH ⁵⁰, M. KOWALSKI ^{10,64}, T. KOZYNETS²², K. KRUISWIJK³⁸,
E. KRUPCZAK²⁴, A. KUMAR ⁶⁴, E. KUN¹¹, N. KURAHASHI ⁵⁰, N. LAD⁶⁴, C. LAGUNAS GUALDA ⁶⁴,
M. LAMOUREUX ³⁸, M. J. LARSON ¹⁹, F. LAUBER ⁶³, J. P. LAZAR ^{14,41}, J. W. LEE ⁵⁷,
K. LEONARD DEHOLTON ^{60,61}, A. LESZCZYŃSKA ⁴⁵, M. LINCETTO¹¹, Q. R. LIU ⁴¹, M. LIUBARSKA²⁵, E. LOHFINK⁴²,
C. LOVE⁵⁰, C. J. LOZANO MARISCAL⁴⁴, L. LU ⁴¹, F. LUCARELLI ²⁸, A. LUDWIG ³⁷, W. LUSZCZAK ^{20,21}, Y. LYU ^{8,9},
J. MADSEN ⁴¹, K. B. M. MAHN²⁴, Y. MAKINO⁴¹, E. MANAO⁶⁵, S. MANCINA^{41,49}, W. MARIE SAINTE⁴¹, I. C. MARIŞ ¹²,
S. MARKA⁴⁷, Z. MARKA⁴⁷, M. MARSEE⁵⁹, I. MARTINEZ-SOLER¹⁴, R. MARUYAMA ⁴⁶, F. MAYHEW²⁴, T. MCELROY²⁵,
F. McNALLY ³⁹, J. V. MEAD²², K. MEAGHER ⁴¹, S. MECHBAL⁶⁴, A. MEDINA²¹, M. MEIER ¹⁶, Y. MERCKX¹³,
L. MERTEN ¹¹, J. MICALLEF²⁴, T. MONTARULI ²⁸, R. W. MOORE ²⁵, Y. MORII¹⁶, R. MORSE⁴¹, M. MOULAI ⁴¹,
T. MUKHERJEE³¹, R. NAAB ⁶⁴, R. NAGAI ¹⁶, M. NAKOS⁴¹, U. NAUMANN⁶³, J. NECKER ⁶⁴, M. NEUMANN⁴⁴,
H. NIEDERHAUSEN ²⁴, M. U. NISA ²⁴, A. NOELL¹, S. C. NOWICKI²⁴, A. OBERTACKE POLLMANN ¹⁶, V. O'DELL⁴¹,
M. OEHLER³¹, B. OEYEN ²⁹, A. OLIVAS¹⁹, R. ORSOE⁶⁵, J. OSBORN⁴¹, E. O'SULLIVAN ⁶², H. PANDYA ⁴⁵, N. PARK ³³,
G. K. PARKER⁴, E. N. PAUDEL ⁴⁵, L. PAUL⁴³, C. PÉREZ DE LOS HEROS ⁶², J. PETERSON⁴¹, S. PHILIPPEN ¹,
S. PIEPER⁶³, A. PIZZUTO ⁴¹, M. PLUM ⁵¹, A. PONTÉN⁶², Y. POPOVYCH⁴², M. PRADO RODRIGUEZ⁴¹, B. PRIES ²⁴,
R. PROCTER-MURPHY¹⁹, G. T. PRZYBYLSKI⁹, J. RACK-HELLES⁴², K. RAWLINS³, Z. RECHAV⁴¹, A. REHMAN ⁴⁵,
P. REICHERTZ¹¹, G. RENZI¹², E. RESCONI ⁶⁵, S. REUSCH⁶⁴, W. RHODE ²³, M. RICHMAN⁵⁰, B. RIEDEL ⁴¹,
E. J. ROBERTS², S. ROBERTSON^{8,9}, S. RODAN⁵⁷, G. ROELLINGHOFF⁵⁷, M. RONGEN ⁴², C. ROTT ^{54,57}, T. RUHE²³,
L. RUOHAN⁶⁵, D. RYCKBOSCH²⁹, I. SAFA ^{14,41}, J. SAFFER³², D. SALAZAR-GALLEGOS ²⁴, P. SAMPATHKUMAR³¹,
S. E. SANCHEZ HERRERA²⁴, A. SANDROCK ²³, M. SANTANDER ⁵⁹, S. SARKAR ²⁵, S. SARKAR ⁴⁸, J. SAVELBERG¹,
P. SAVINA⁴¹, M. SCHAUFEL¹, H. SCHIELER ³¹, S. SCHINDLER ²⁶, B. SCHLÜTER⁴⁴, F. SCHLÜTER ¹², T. SCHMIDT¹⁹,
J. SCHNEIDER ²⁶, F. G. SCHRÖDER ^{31,45}, L. SCHUMACHER ⁶⁵, G. SCHWEFER¹, S. SCLAFANI ⁵⁰, D. SECKEL⁴⁵,
S. SEUNARINE ⁵², R. SHAH⁵⁰, A. SHARMA⁶², S. SHEFALI³², N. SHIMIZU¹⁶, M. SILVA ⁴¹, B. SKRZYPEK ¹⁴,
B. SMITHERS ⁴, R. SNIHUR⁴¹, J. SOEDINGREKSO²³, A. SØGAARD²², D. SOLDIN ³², G. SOMMANI ¹¹, C. SPANNFELLNER⁶⁵

G. M. SPICZAK ⁵², C. SPIERING ⁶⁴, M. STAMATIKOS,²¹ T. STANEV,⁴⁵ T. STEZELBERGER ⁹, T. STÜRWARD,⁶³
 T. STUTTARD ²², G. W. SULLIVAN ¹⁹, I. TABOADA ⁶, S. TER-ANTONYAN ⁷, M. THIESMEYER,¹
 W. G. THOMPSON ¹⁴, J. THWAITES,⁴¹ S. TILAV,⁴⁵ K. TOLLEFSON ²⁴, C. TÖNNIS,⁵⁷ S. TOSCANO ¹², D. TOSI,⁴¹
 A. TRETTIN,⁶⁴ C. F. TUNG ⁶, R. TURCOTTE,³¹ J. P. TWAGIRAYEZU,²⁴ B. TY,⁴¹ M. A. UNLAND ELORRIETA ⁴⁴,
 A. K. UPADHYAY,^{41,*} K. UPSHAW,⁷ N. VALTONEN-MATTILA ⁶², J. VANDENBROUCKE ⁴¹, N. VAN EIJDHOVEN ¹³,
 D. VANNEROM,¹⁵ J. VAN SANTEN ⁶⁴, J. VARA,⁴⁴ J. VEITCH-MICHAELIS,⁴¹ M. VENUGOPAL,³¹ S. VERPOEST ²⁹,
 D. VESKE,⁴⁷ C. WALCK,⁵⁵ T. B. WATSON ⁴, C. WEAVER ²⁴, P. WEIGEL,¹⁵ A. WEINDL,³¹ J. WELDERT,^{60,61}
 C. WENDT ⁴¹, J. WERTHEBACH,²³ M. WEYRAUCH,³¹ N. WHITEHORN ^{24,37}, C. H. WIEBUSCH ¹, N. WILLEY,²⁴
 D. R. WILLIAMS,⁵⁹ A. WOLF,¹ M. WOLF ⁶⁵, G. WREDE,²⁶ X. W. XU,⁷ J. P. YANEZ,²⁵ E. YILDIZCI,⁴¹ S. YOSHIDA ¹⁶,
 F. YU,¹⁴ S. YU,²⁴ T. YUAN ⁴¹, Z. ZHANG,⁵⁶ AND P. ZHELNIN¹⁴

¹*III. Physikalisches Institut, RWTH Aachen University, D-52056 Aachen, Germany*

²*Department of Physics, University of Adelaide, Adelaide, 5005, Australia*

³*Dept. of Physics and Astronomy, University of Alaska Anchorage, 3211 Providence Dr., Anchorage, AK 99508, USA*

⁴*Dept. of Physics, University of Texas at Arlington, 502 Yates St., Science Hall Rm 108, Box 19059, Arlington, TX 76019, USA*

⁵*CTSPS, Clark-Atlanta University, Atlanta, GA 30314, USA*

⁶*School of Physics and Center for Relativistic Astrophysics, Georgia Institute of Technology, Atlanta, GA 30332, USA*

⁷*Dept. of Physics, Southern University, Baton Rouge, LA 70813, USA*

⁸*Dept. of Physics, University of California, Berkeley, CA 94720, USA*

⁹*Lawrence Berkeley National Laboratory, Berkeley, CA 94720, USA*

¹⁰*Institut für Physik, Humboldt-Universität zu Berlin, D-12489 Berlin, Germany*

¹¹*Fakultät für Physik & Astronomie, Ruhr-Universität Bochum, D-44780 Bochum, Germany*

¹²*Université Libre de Bruxelles, Science Faculty CP230, B-1050 Brussels, Belgium*

¹³*Vrije Universiteit Brussel (VUB), Dienst ELEM, B-1050 Brussels, Belgium*

¹⁴*Department of Physics and Laboratory for Particle Physics and Cosmology, Harvard University, Cambridge, MA 02138, USA*

¹⁵*Dept. of Physics, Massachusetts Institute of Technology, Cambridge, MA 02139, USA*

¹⁶*Dept. of Physics and The International Center for Hadron Astrophysics, Chiba University, Chiba 263-8522, Japan*

¹⁷*Department of Physics, Loyola University Chicago, Chicago, IL 60660, USA*

¹⁸*Dept. of Physics and Astronomy, University of Canterbury, Private Bag 4800, Christchurch, New Zealand*

¹⁹*Dept. of Physics, University of Maryland, College Park, MD 20742, USA*

²⁰*Dept. of Astronomy, Ohio State University, Columbus, OH 43210, USA*

²¹*Dept. of Physics and Center for Cosmology and Astro-Particle Physics, Ohio State University, Columbus, OH 43210, USA*

²²*Niels Bohr Institute, University of Copenhagen, DK-2100 Copenhagen, Denmark*

²³*Dept. of Physics, TU Dortmund University, D-44221 Dortmund, Germany*

²⁴*Dept. of Physics and Astronomy, Michigan State University, East Lansing, MI 48824, USA*

²⁵*Dept. of Physics, University of Alberta, Edmonton, Alberta, Canada T6G 2E1*

²⁶*Erlangen Centre for Astroparticle Physics, Friedrich-Alexander-Universität Erlangen-Nürnberg, D-91058 Erlangen, Germany*

²⁷*Physik-Department, Technische Universität München, D-85748 Garching, Germany*

²⁸*Département de physique nucléaire et corpusculaire, Université de Genève, CH-1211 Genève, Switzerland*

²⁹*Dept. of Physics and Astronomy, University of Gent, B-9000 Gent, Belgium*

³⁰*Dept. of Physics and Astronomy, University of California, Irvine, CA 92697, USA*

³¹*Karlsruhe Institute of Technology, Institute for Astroparticle Physics, D-76021 Karlsruhe, Germany*

³²*Karlsruhe Institute of Technology, Institute of Experimental Particle Physics, D-76021 Karlsruhe, Germany*

³³*Dept. of Physics, Engineering Physics, and Astronomy, Queen's University, Kingston, ON K7L 3N6, Canada*

³⁴*Department of Physics & Astronomy, University of Nevada, Las Vegas, NV, 89154, USA*

³⁵*Nevada Center for Astrophysics, University of Nevada, Las Vegas, NV 89154, USA*

³⁶*Dept. of Physics and Astronomy, University of Kansas, Lawrence, KS 66045, USA*

³⁷*Department of Physics and Astronomy, UCLA, Los Angeles, CA 90095, USA*

³⁸*Centre for Cosmology, Particle Physics and Phenomenology - CP3, Université catholique de Louvain, Louvain-la-Neuve, Belgium*

³⁹*Department of Physics, Mercer University, Macon, GA 31207-0001, USA*

⁴⁰*Dept. of Astronomy, University of Wisconsin-Madison, Madison, WI 53706, USA*

⁴¹*Dept. of Physics and Wisconsin IceCube Particle Astrophysics Center, University of Wisconsin-Madison, Madison, WI 53706, USA*

⁴²*Institute of Physics, University of Mainz, Staudinger Weg 7, D-55099 Mainz, Germany*

⁴³*Department of Physics, Marquette University, Milwaukee, WI, 53201, USA*

⁴⁴*Institut für Kernphysik, Westfälische Wilhelms-Universität Münster, D-48149 Münster, Germany*

⁴⁵*Bartol Research Institute and Dept. of Physics and Astronomy, University of Delaware, Newark, DE 19716, USA*

⁴⁶*Dept. of Physics, Yale University, New Haven, CT 06520, USA*

- ⁴⁷ *Columbia Astrophysics and Nevis Laboratories, Columbia University, New York, NY 10027, USA*
- ⁴⁸ *Dept. of Physics, University of Oxford, Parks Road, Oxford OX1 3PU, UK*
- ⁴⁹ *Dipartimento di Fisica e Astronomia Galileo Galilei, Università Degli Studi di Padova, 35122 Padova PD, Italy*
- ⁵⁰ *Dept. of Physics, Drexel University, 3141 Chestnut Street, Philadelphia, PA 19104, USA*
- ⁵¹ *Physics Department, South Dakota School of Mines and Technology, Rapid City, SD 57701, USA*
- ⁵² *Dept. of Physics, University of Wisconsin, River Falls, WI 54022, USA*
- ⁵³ *Dept. of Physics and Astronomy, University of Rochester, Rochester, NY 14627, USA*
- ⁵⁴ *Department of Physics and Astronomy, University of Utah, Salt Lake City, UT 84112, USA*
- ⁵⁵ *Oskar Klein Centre and Dept. of Physics, Stockholm University, SE-10691 Stockholm, Sweden*
- ⁵⁶ *Dept. of Physics and Astronomy, Stony Brook University, Stony Brook, NY 11794-3800, USA*
- ⁵⁷ *Dept. of Physics, Sungkyunkwan University, Suwon 16419, Korea*
- ⁵⁸ *Institute of Physics, Academia Sinica, Taipei, 11529, Taiwan*
- ⁵⁹ *Dept. of Physics and Astronomy, University of Alabama, Tuscaloosa, AL 35487, USA*
- ⁶⁰ *Dept. of Astronomy and Astrophysics, Pennsylvania State University, University Park, PA 16802, USA*
- ⁶¹ *Dept. of Physics, Pennsylvania State University, University Park, PA 16802, USA*
- ⁶² *Dept. of Physics and Astronomy, Uppsala University, Box 516, S-75120 Uppsala, Sweden*
- ⁶³ *Dept. of Physics, University of Wuppertal, D-42119 Wuppertal, Germany*
- ⁶⁴ *Deutsches Elektronen-Synchrotron DESY, Platanenallee 6, 15738 Zeuthen, Germany*
- ⁶⁵ *Physik-department, Technische Universität München, D-85748 Garching, Germany*

ABSTRACT

We present a catalog of likely astrophysical neutrino track-like events from the IceCube Neutrino Observatory. IceCube began reporting likely astrophysical neutrinos in 2016 and this system was updated in 2019. The catalog presented here includes events that were reported in real-time since 2019, as well as events identified in archival data samples starting from 2011. We report 275 neutrino events from two selection channels as the first entries in the catalog, the IceCube Event Catalog of Alert Tracks, which will see ongoing extensions with additional alerts. The Gold and Bronze alert channels respectively provide neutrino candidates with 50% and 30% probability of being astrophysical, on average assuming an astrophysical neutrino power law energy spectral index of 2.19. For each neutrino alert, we provide the reconstructed energy, direction, false alarm rate, probability of being astrophysical in origin, and likelihood contours describing the spatial uncertainty in the alert’s reconstructed location. We also investigate a directional correlation of these neutrino events with gamma-ray and X-ray catalogs including 4FGL, 3HWC, TeVCat and Swift-BAT.

1. INTRODUCTION

The emerging field of multimessenger astronomy combines measurements taken across the electromagnetic spectrum with neutrinos and gravitational waves to elucidate the nature of astrophysical objects. Notable examples of discoveries in recent years include the joint gravitational wave and electromagnetic observation of a binary neutron star merger (Abbott et al. 2017), and the coincident detection of neutrinos and gamma rays from the blazar TXS 0506+056 (Aartsen et al. 2018a). Breakthroughs like the latter hold the key to identifying the sites of hadronic acceleration and solving a major open puzzle in modern astrophysics, the origin of cosmic rays. Astrophysical neutrinos are produced in either pp collisions or $p\gamma$ interactions following cosmic-ray acceleration, and neutrino observatories like IceCube have a unique role in probing the distant universe in the TeV–PeV energy regime. The prompt observation of transient phenomena, such as gamma-ray bursts, tidal disruption events, and supernovae, in different wavelengths and messengers requires the rapid sharing of information between different observational facilities. Since 2016, IceCube has been issuing real-time alerts within minutes of the detection of astrophysical neutrino candidates (Aartsen et al. 2017a). Several improvements were introduced in the real-time stream in 2019 (Blaufuss et al. 2020). The updated program includes increased signal purity, better rejection of backgrounds, and an expanded alert selection resulting in more frequent alerts from IceCube than the previous alert program. These improvements also introduced a two-level

* also at Institute of Physics, Sachivalaya Marg, Sainik School Post, Bhubaneswar 751005, India

† also at Department of Space, Earth and Environment, Chalmers University of Technology, 412 96 Gothenburg, Sweden

‡ also at Earthquake Research Institute, University of Tokyo, Bunkyo, Tokyo 113-0032, Japan

classification of signal purity in the form of “Gold” and “Bronze” alerts. In this work, we describe the improvements made to the real-time alert selection, apply the updated selection to archival IceCube data going back to 2011 when IceCube first began full operations with 86 strings, and present the first catalog of neutrino events of likely astrophysical origin. This catalog, the IceCube Event Catalog of Alert Tracks (ICECAT-1), contains detailed information on key parameters of 275 neutrino events detected between 13 May 2011 and 31 December 2020, providing a unique sample for multimessenger studies. The accompanying data release provides the log-likelihood sky-maps and spatial uncertainties for all events. This will also establish a framework for continued data releases from future alerts, including additions from the most recent IceCube alerts.

This paper is structured as follows. We introduce the IceCube Neutrino Observatory and real-time data selection for this catalog in Section 2. In Section 3, we describe how the alert events are further processed and prepared for follow-ups. We discuss the overall properties of the catalog in Section 4. We describe a potential search for correlations with a few multi-wavelength catalogs in Section 5, and conclude in section 6.

2. DETECTOR AND EVENT SELECTION

The IceCube Neutrino Observatory consists of 86 strings of photo-detectors embedded in a cubic kilometer of ice beneath the South Pole. The photo-detectors, known as digital optical modules (DOMs), are spaced along the vertical length of each string (Abbasi et al. 2009). The strings are arranged on average 125 m apart in a hexagonal grid with a more densely instrumented set of strings located in the center of the array is known as DeepCore (Abbasi et al. 2012). In addition to the in-ice detectors, there is also a surface array of 162 ice-filled tanks instrumented with two DOMs each, known as IceTop (Abbasi et al. 2013). The surface array functions as a detector for air showers induced by cosmic rays and gamma rays.

IceCube detects the Cherenkov light produced by the secondary charged particles from neutrino interactions propagating through the ice. The total number of photo-electrons (PE) detected (deposited charge) and their arrival times are used to reconstruct the deposited energy and the incoming direction of these charged particles. The optical emission signatures can be classified into two distinct types of event morphologies: tracks and cascades. Track-like events are predominantly produced by muons, which originate in charge-current (CC) interactions of muon neutrinos and from cosmic-ray-induced showers. At final selection level, the majority of muon track-like events detected pass fully through the instrumented volume; however, tracks starting or stopping within the instrumented volume are observed. Starting tracks in particular, generated by a muon neutrino CC interaction within the IceCube instrumented volume can be a strong indication of astrophysical origin Abbasi et al. (2021a). The directions of such events can be reconstructed with an uncertainty of less than 1° Aartsen et al. (2014a). The location of the neutrino interaction, which can be $\mathcal{O}(\text{km})$ outside the instrumented volume, and the length of the track captured within the detector can lead to large uncertainties in the measured neutrino energy. Cascades are produced by all-flavor neutral-current (NC) neutrino interactions as well as electron-neutrino CC interactions. These events deposit all their energy within spherical showers of $\mathcal{O}(10)$ m and can only be resolved with angular uncertainties of $\sim 10^\circ$ (Aartsen et al. 2014a; Abbasi et al. 2021b). Additionally, cascade-like signatures can arise from charge-current interactions of tau neutrinos Aartsen et al. (2020a) or from neutrinos at the Glashow resonance Aartsen et al. (2021). Tracks – due to their superior angular resolution – are best suited for use in multimessenger searches for astrophysical sources, and are the primary constituents of IceCube real-time alerts. In July 2020, IceCube also began issuing alerts for cascade-like events¹. However, the cascade sample is not part of the catalog in this paper.

2.1. Real-time Reconstruction and Communication

IceCube detects neutrinos at a rate of a few mHz, the vast majority of which are atmospheric neutrinos produced in cosmic-ray interactions in the Earth’s atmosphere (Abbasi et al. 2011; Aartsen et al. 2015). A real-time infrastructure identifies events with a significant probability of being of astrophysical origin (neutrino energy $>\sim 100$ TeV) and promptly alerts the astronomy community to such a detection. The system is described in detail in Aartsen et al. (2017b). We discuss it briefly here with an emphasis on updates and improvements relevant for this catalog.

An online filtering system at the South Pole identifies candidate neutrino events. The candidate events are reconstructed on several hundred parallel filter clients to determine their observed energies, directions, and morphology. Additional selection criteria (Aartsen et al. (2017b)) are applied to determine whether an event passes the preliminary

¹ https://gcn.gsfc.nasa.gov/amon_icecube_cascade_events.html

online alert criteria. A single online alert writer process collates these events for transmission to I3Live – the IceCube experiment control system (Aartsen et al. 2017a). The key event summary data for candidate events passing the quality cuts are relayed to the IceCube data center in the Northern hemisphere over satellite. The full event information including the signals registered by the DOMs follows in a second message that is used for a detailed follow-up reconstructions as explained in section 3.

A dedicated computing system, located at the IceCube data center in the Northern hemisphere, further evaluates the alert candidates arriving from the South Pole to check if they pass the online alert criteria. If selected, an alert message is generated and distributed to the public through the Astrophysical Multimessenger Observatory Network (AMON) system (Ayala Solares et al. 2020) which utilizes the General Coordinates Network² (GCN) for communication. The whole chain of events, from the neutrino detection to the issuance of an alert is fully automated and takes between 30 s to 40 s on average.

2.2. Updated Event Selections

The updated event selection introduced in 2019 includes two key improvements that aim to convey the detection of potential astrophysical tracks to the community as frequently as possible. One is the introduction of “Gold” and “Bronze” streams that classify alerts based on their likelihood of being astrophysical in nature. The classification is based on a quantity called “signalness,” which is defined as,

$$\text{Signalness}(E, \delta) = \frac{N_{\text{signal}}(E, \delta)}{N_{\text{signal}}(E, \delta) + N_{\text{background}}(E, \delta)}. \quad (1)$$

Here E is the reconstructed event energy, δ is the event declination, $N_{\text{signal}}(E, \delta)$ and $N_{\text{background}}(E, \delta)$ are the expected number of signal and background events at declination δ and above energy E determined from simulations. $N_{\text{signal}}(E, \delta)$ and $N_{\text{background}}(E, \delta)$, and therefore signalness are functions of the assumed astrophysical neutrino spectrum. The streams were optimized on simulations using an astrophysical neutrino spectrum of $E^{-2.19}$ (Haack & Wiebusch 2017). The signalness quantity assigns a probability of being an astrophysical neutrino to each alert event, assuming the same $E^{-2.19}$ astrophysical neutrino spectrum. The alert generation criteria are optimized such that “Bronze” alerts have an average signalness value between 30 % and 50 %, whereas “Gold” candidates have an average signalness above 50%. Thus, the Gold stream has a higher signal purity. We note that the signalness is calculated after event selection to grade alerts, and is not explicitly used in alert selection. Certain tracks with high signalness values may not pass the real-time criteria and would end up in other selections. The signalness of each alert is sent out as part of the GCN notice. The “notice type” field indicates the Bronze (Gold) alerts as ICECUBE Astrotrack Bronze (Gold). An example of a GCN notice for IC190730A can be seen at the following URL https://gcn.gsfc.nasa.gov/notices_amon_g_b/132910.57145925.amon.

The second improvement to the updated event selection is the introduction of a new track selection known as Gamma-ray Follow-Up (GFU) selection. This complements the previously existing selections in the real-time scheme. The event selections are summarized below.

2.2.1. Gamma-Ray Followup Event Selection

This event selection is based on an existing IceCube data neutrino candidate selection that was originally designed to provide triggers for follow-up by Imaging Air Cherenkov Telescopes in gamma rays – hence the name Gamma-ray Followup or GFU (Aartsen et al. 2016a). This reconstruction targets through-going tracks and employs separate boosted decision tree-based selections for events from the Northern and Southern hemisphere (up-going and down-going events in the IceCube reference frame, respectively) to suppress atmospheric backgrounds. A threshold is applied to the reconstructed event energy to achieve the 30% and 50% signalness criteria for alerts. This results in only the highest energy events (hundreds of TeV) being selected. Figure 1 shows the effective area for the GFU Gold and Bronze alert selection as a function of neutrino energy. The majority (86%) of the alerts issued by IceCube fall under the GFU selection. The ten-year catalog includes 72 GFU Gold and 164 GFU Bronze events.

² <https://gcn.nasa.gov/>

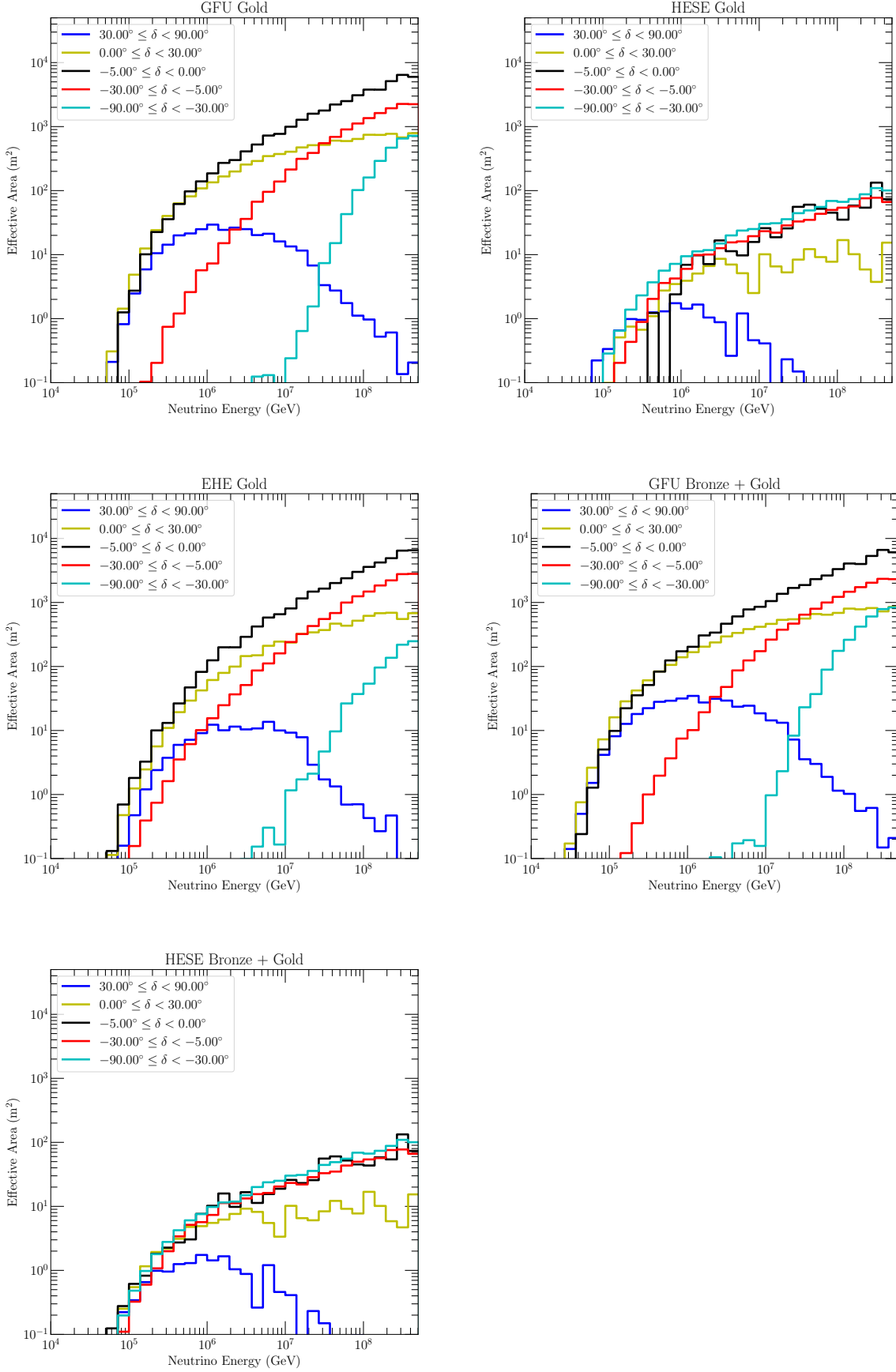


Figure 1. The $\nu_\mu + \bar{\nu}_\mu$ effective areas for the event selections used in this catalog as a function of neutrino energy. The solid lines show the effective area in different declination bands: $[30^\circ, 90^\circ]$ (blue), $[0^\circ, 30^\circ]$ (yellow), $[-5^\circ, 0^\circ]$ (black), $[-30^\circ, -5^\circ]$ (red) and $[-90^\circ, -30^\circ]$ (cyan).

2.2.2. High-Energy Starting Event Selection

The High-Energy Starting Event (HESE) selection for alerts includes only starting tracks, track-like events that have the neutrino interaction vertex inside the fiducial volume of the detector (Abbasi et al. 2021a). This technique efficiently rejects the atmospheric muon background (Aartsen et al. 2013). Since, the highest energy events are more likely to be of astrophysical origin, only the events that have a total deposited charge in the detector of at least 6000 photoelectrons are considered. As an improvement to previous HESE alerts Aartsen et al. (2017b), additional cuts are introduced to further reduce poorly reconstructed event. We only use events that have a minimum measured track length of 200 m. Due to the effective veto requirement for HESE alerts, down-going events from the Southern hemisphere can be observed at lower neutrino energies, as illustrated by the HESE effective area for different declination bins in Fig. 1. The ten-year catalog includes 9 HESE Gold and 8 HESE Bronze events.

2.2.3. Extremely High-Energy Event Selection

The Extremely High-Energy Event (EHE) selection is optimized for detecting track-like neutrino events with energies between 500 TeV and 10 PeV. Atmospheric backgrounds are minimized by employing a two dimensional cut in the plane of the reconstructed zenith angle and the logarithm of the deposited charge detected. The selection is unchanged from the one described in Aartsen et al. (2017b), and the cuts are set to achieve an average signalness of 50%, and therefore EHE events are only sent as part of the Gold stream. Figure 1 shows the effective area for the EHE selection as a function of neutrino energy. This catalog contains 22 events that passed the EHE selection during the 9.6-year period.

2.3. Expected and Observed Rates

Figure 2 shows the time-evolution of the number of observed alerts over the years. The cumulative number of total alerts, as a function of year are best described by a straight line with slope 28.6 alerts per year. Table 1 shows the number of expected and observed number of events in the 3,514 days of the IceCube data used in this work. We calculate the expected number of alerts arising from astrophysical sources for each selection by multiplying its respective effective area with IceCube’s latest measured diffuse astrophysical muon neutrino spectrum (Abbasi et al. 2022a) that reports a spectral power-law index of 2.37. Since, the event selection was originally optimized assuming a spectral index of 2.19 based on a previous IceCube measurement (Haack & Wiebusch 2017), the numbers reported here slightly differ from the ones in Blaufuss et al. (2020). IceCube continues to take data and refine its reconstruction methods resulting in a more precise measurement of the astrophysical neutrino spectrum over the years. This evolution is reflected in the use of an updated spectral index in this work. The expected number of signal events can change up to $\sim 15\%$ when using a spectral index of 2.19 instead of 2.37. The expected number of background events is calculated using a simulation of atmospheric muons and neutrinos (Schönert et al. 2009; Heck et al. 1998). We also note that the event selections are not mutually exclusive – a single event may pass multiple selections. In particular, GFU and EHE selections have significant overlap as they both focus on through-going tracks. The expected numbers in Table 1, account for the overlap and only report the unique events from each stream. In real-time, if an event passes multiple selections only one alert is issued based on a hierarchical rule for labeling. The hierarchical scheme in order of preference for the Gold stream is GFU Gold, EHE Gold and HESE Gold. Similarly, for the Bronze stream, a GFU Bronze alert is sent preferentially over a HESE Bronze alert. An event passing both the Gold and Bronze selections is only sent in the Gold stream. The preference order is decided based on the angular resolutions and relative signal purity of the different streams.

The observed rates of alerts from the Gold and Bronze channels shown in Table 1 are compatible with expectations when considering Poisson fluctuations as well as the uncertainties in the astrophysical neutrino spectral parameters and the background modeling. For instance, considering the errors on the measured diffuse muon neutrino spectral parameters (Abbasi et al. 2022a), the expected number of GFU Gold signal events can be as low as 39.1, bringing the overall expected rate from 101.3 to 86.1, which is within $\sim 1.5\sigma$ of the observed number of 72 events. It should be noted that while the average signalness of the Gold and Bronze selection, as shown in Figure 5, generally agree with the 50% and 30% targets, the overall mix of signal and background events are different. This arises from the differing signal and background energy distributions near the selection threshold. Overall, the HESE Gold stream has the highest average signal purity of $\sim 57\%$.

In addition to overall rates for each alert type, we also calculate the false alarm rate (FAR) on an event-by-event basis. The FAR for a given alert gives the annual rate of background events in IceCube with a direction and energy similar to the issued alert, and is derived from $N_{\text{background}}(E, \delta)$ used in the signalness calculation.

Table 1. The number of expected signal and background events, and the total observed events for each alert stream in ~ 9.6 years of the catalog live time. The expected number of events are calculated for the best-fit diffuse muon neutrino flux (Abbasi et al. 2022a) with a spectral index of 2.37.

Event Type	Expected Signal	Expected Background	Total Expected	Total Observed
GFU Gold	54.3	47	101.3	72
GFU Bronze	40.2	138	178.2	164
HESE Gold	5.3	4	9.3	9
HESE Bronze	1.6	9	10.6	8
EHE Gold	3.9	19	22.9	22

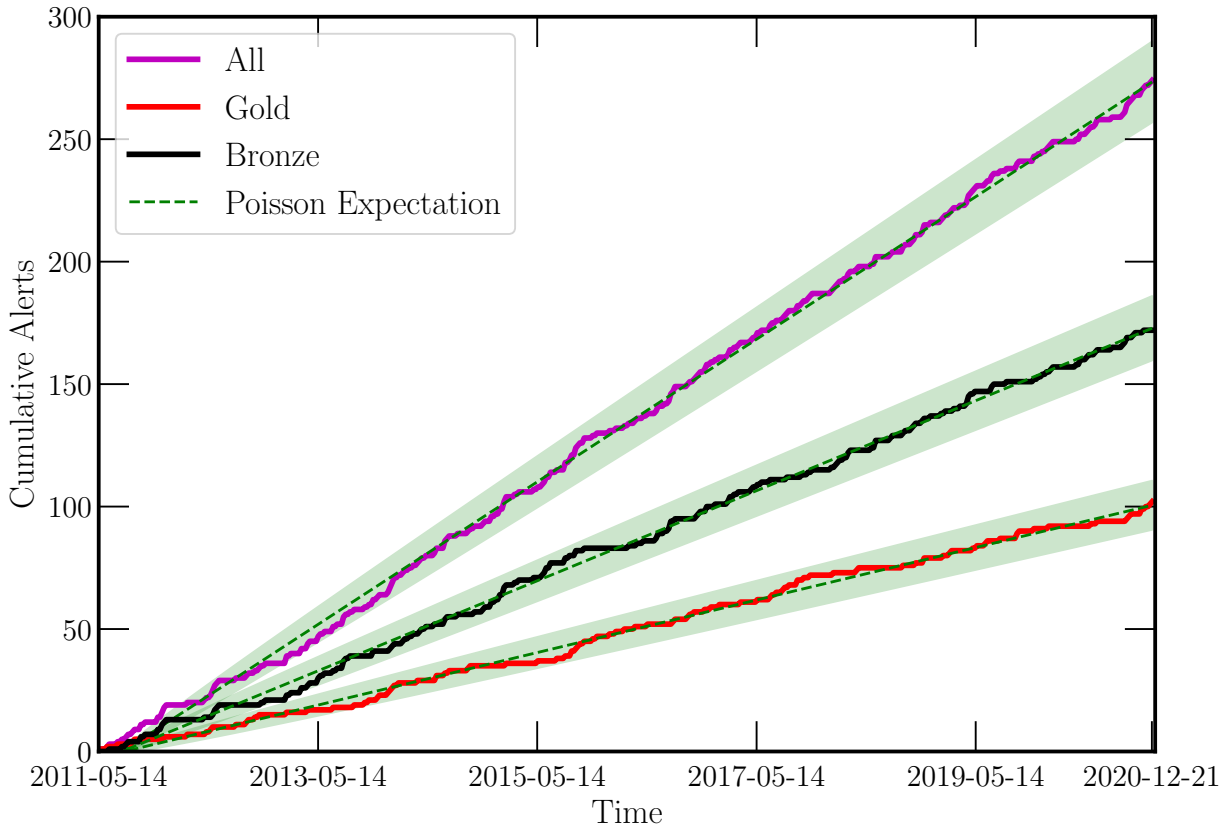


Figure 2. The cumulative number of alerts as a function of time. The solid black and red lines show the number of Gold and Bronze alerts respectively, while the magenta line shows the combined number for all alerts. The dashed green line and the shaded green band show the median and standard deviation of the best-fit Poisson distribution to the number of alerts in each category.

3. ALERT PROCESSING AND FOLLOW-UPS

Due to computational limitations at the South Pole experimental site, and the need for promptly issuing an alert, the online reconstruction cannot utilize complex, computationally-intensive algorithms. Once all the event information has been transmitted to the North, a more refined set of follow-up reconstructions based on Aartsen et al. (2014a) begin on a computing cluster. The follow-up reconstruction consists of a maximum-likelihood based scan of the entire sky to search for an event direction consistent with the signals registered by the DOMs. We bin the sky into two-dimensional grids of increasing resolution in steps following the HEALPix pixelization scheme (Górski et al. 2005). Each pixel defines a potential event direction in right ascension and declination. At each step, in each pixel, we fix the event direction and compute the likelihood of the best-fit deposited energy and the neutrino interaction position. Repeating the procedure over all pixels yields a likelihood map of the sky. The pixel corresponding to the maximum likelihood defines the best-fit direction of the neutrino event. The scans are first performed on a coarse grid with NSIDE = 8, corresponding to a mean pixel spacing of 7.3° . The best-fit pixels are selected for the next steps with finer scans with NSIDES 64 (pixel size 0.9°) and 1024 (pixel size 0.06°). Each sky scan takes between one to three hours, yielding an improved angular reconstruction over the initial alert. In order to ensure that the reconstruction converges to a global minimum, at each step, we test several positional variations iteratively by using the result of a regular fit as a seed for the next iteration. If there are multiple local minima, the repeated iterations ensure that at least one of the results is a global minimum.

The angular uncertainty contours at 50% and 90% confidence level are extracted using predefined values of change in log-likelihood based on simulated neutrino events to ensure the required coverage (Aartsen et al. 2018b). In order to cover potential systematic errors from detector uncertainties (such as glacial ice optical parameters), the detector systematic parameters were varied within expected errors during the simulation of the neutrino events used to determine the contour levels. As described in Aartsen et al. (2018b), we simulate an ensemble of events with similar energy deposition and position in the detector as IC160427A (Kankare et al. 2019), varying the ice model parameters (Abbasi et al. 2022b) in each simulation. The simulated events are reconstructed, and the log-likelihoods of their reconstructed directions are compared to the log-likelihoods of their true directions. This procedure yields a distribution of change in log-likelihood which folds in the systematic uncertainties, and is used to extract the error contours. We note that the calibration of the change in log-likelihood is especially sensitive to the optical properties of the ice, an area of intense study within IceCube (Abbasi et al. 2021c). While these results represent our current modeling, updated parameters and reconstructions for alert candidates will be released as catalog updates as they become available. In real-time operations, the results from the follow-up scan are disseminated via a GCN circular and a revised GCN notice. In particular, the notice includes the circularized error region based on the follow-up reconstruction. An example of the revised GCN notice for the event IC190730A can be seen at this URL <https://gcn.gsfc.nasa.gov/gcn3/25225.gcn3>.

For the compilation of the catalog, the same sky scan is performed on the selected alerts from the archival IceCube data on a commercial cloud computing service. Figure 3 illustrates the result of one such scan, for an example alert from the catalog, IC150119. In addition, we also apply a convolutional neural network (CNN) based classifier to better distinguish the morphology of each event (Kronmueller & Glauch 2019). Each event is assigned a score between 0 and 1 for how well it fits the following four hypotheses: cascade, skimming event (primary vertex outside the detector and no energy deposited within), starting track (interaction vertex inside the detector volume) or stopping track (track length of less than ~ 1500 m). In this work, we provide the complete likelihood maps and the uncertainty contours, as described above, for all the alerts in the accompanying data release.

3.1. *IceTop Veto*

Recently, 21 Oct 2022, we introduced an additional veto mechanism to reject atmospheric muons that may pass the alert selection criteria. This veto makes use of the IceTop surface array to search for cosmic-ray-induced showers accompanying a track-like event in the in-ice detector (Amin 2021). This is particularly useful in the case of down-going air showers inclined at an angle, typically below 82° with respect to the zenith, that pass through IceCube and where the reconstructed track is not fully contained in the IceTop detector footprint. The IceTop veto criteria look for a threshold number of coincident pulses in IceTop tanks during a $1 \mu\text{s}$ time-window (Amin 2021). Since the criteria were developed after the compilation of the catalog, we do not discard the vetoed alerts but mark them as such. The probability that the veto algorithm incorrectly rejects a true astrophysical neutrino event is $\sim 10^{-4}$.

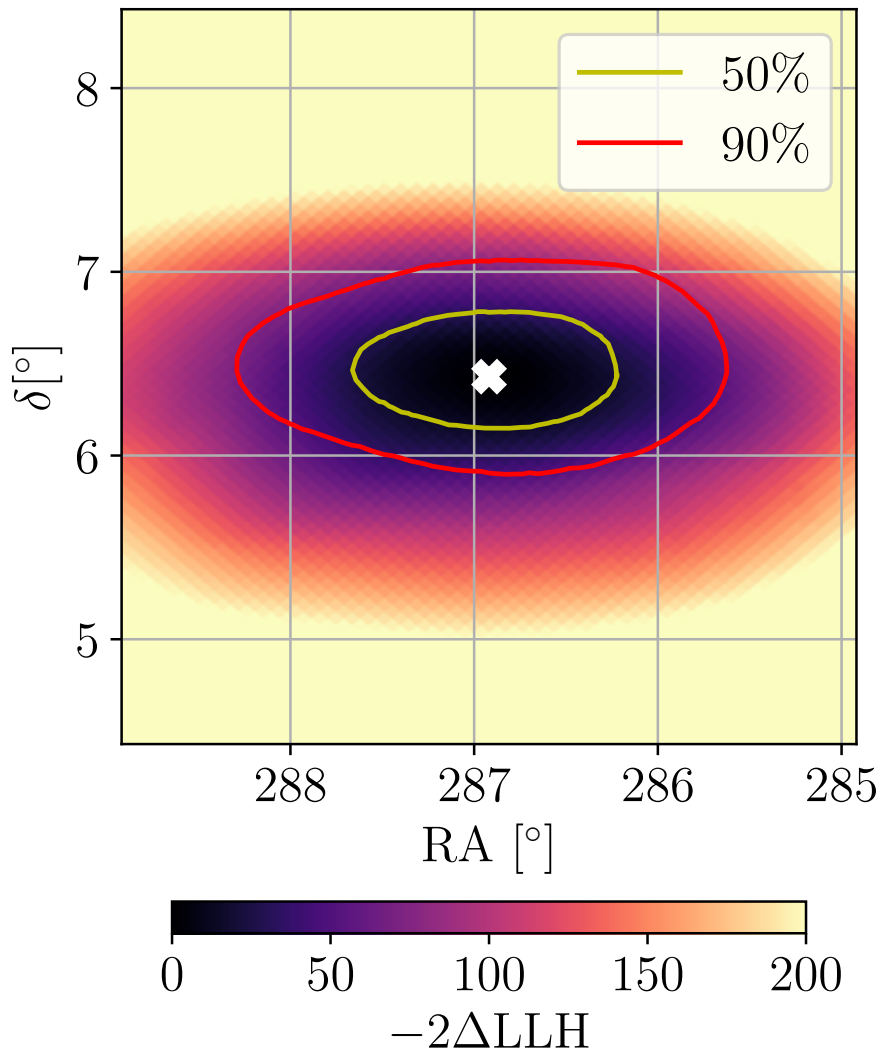


Figure 3. The result of the sky scan shown in likelihood space for IC150119. The best-fit position of the event is noted by the white cross in the center where the likelihood is maximized. The yellow and red contours denote the uncertainty in the location as the 50% and 90% confidence level changes in the likelihood (see section 3). A rectangle that contains the 90% error contour is used to report the +/- errors on the alert location (see Table 3).

4. CATALOG PROPERTIES

We compile the neutrino alert catalog by applying the above-mentioned procedures of event selection followed by likelihood scans on IceCube data going back to May 2011. A total of 275 events pass the alert criteria through the end of 2020, including alerts issued in real-time after the updated system was activated in June 2019. Figure 4 shows the location of all the alerts on a sky map in equatorial coordinates. Figure 6 shows the distribution broken down by alert type. The breakdown of the number of alerts by stream and selection is shown in Table 1. Figure 5 shows

the distributions of energies, false alarm rates, and signalness parameters for all the alerts. Table 3 shows all alerts with their best-fit directions and 90% uncertainties (J2000 coordinates), energy (assuming a spectral index of 2.19) and signalness information. The probable neutrino energy for each event is calculated from the observed muon energy (Abbasi et al. 2013). Figure 7 illustrates the spread of true neutrino energies that contribute to a given observed muon energy. The uncertainties on alert directions reported in Table 3 are obtained from the rectangular region bounding the error contours. After the construction of the catalog, we also checked data from IceTop for signatures of cosmic-ray activity that is temporally correlated with each of the alerts. Eight alerts were vetoed by IceTop data as described above. Such alerts are likely to be caused by atmospheric background and are marked with an asterisk (*) in Table 3, but as these veto criteria were added at a later time, these events were not removed from the catalog. These vetoed events are likely not of astrophysical origin, and future real-time alerts will not be issued for events that fail these veto criteria.

The neutrino event selection used in this catalog is designed to select astrophysical event candidates that are likely to provide well-reconstructed directions on the sky. However, this is not the only astrophysical event selection to have been used in IceCube, and several historical catalogs of astrophysical neutrino candidates have been previously released (Aartsen et al. 2018b, 2014b, 2016b; Abbasi et al. 2022a). While several events contained in these previous catalogs are included here, several do not meet the selection criteria used for this real-time alert selection. This does not imply that these events are not potential astrophysical neutrino candidates, but rather that automated event selections can not supply sufficient information to issue alerts automatically. The information included here for these events also represents our updated understanding of these candidates, using the latest calibration, glacial ice modeling, and reconstruction algorithms.

The complete catalog is provided in electronic format on [dataverse³](https://dataverse.harvard.edu/dataset.xhtml?persistentId=doi:10.7910/DVN/SCRUCD) with columns in addition to the ones in table 3 for each event as follows: I3TYPE (event selection type), FAR per year, scores for each CNN classification for event topology, and a CR.VETO flag to mark significant temporally coincident cosmic-ray shower activity with a given alert.

5. SEARCH FOR CORRELATIONS WITH POTENTIAL CANDIDATES FOR ASSOCIATION

Once an IceCube alert is issued, telescopes can begin follow-up observations around the best-fit location of the neutrino event for potential electromagnetic counterparts. Sources lying within the angular uncertainty contours can be probed on different time-scales for transient activity to obtain clues as to the origin of the neutrino. Using a variety of data samples, IceCube continues to conduct searches for long-term neutrino emission and for correlations of neutrino data with known astrophysical objects across different wavelengths (Aartsen et al. 2017c, 2020b; Aartsen et al. 2019; Abbasi et al. 2022c). For the 275 neutrino events in this catalog, we are performing several follow-up analyses that are the subject of on-going and future publications (Abbasi et al. 2022d, 2023). In this work, we report the results of a time-independent search for spatial correlations between the best-fit positions of the alerts and of sources from five catalogs of gamma-ray and X-ray sources.

We use the following catalogs: the 4FGL-DR2 (Abdollahi et al. 2020) and 3FHL (Ajello et al. 2017) catalogs from Fermi-LAT, 3HWC catalog (Albert et al. 2020) from the HAWC observatory, TeVCat (Wakely & Horan 2008), and the *Swift*-BAT catalog of hard X-ray sources (Oh et al. 2018). We note that these catalogs are not completely independent and some of the sources are present in multiple catalogs. For each of the 275 alerts, using the aforementioned catalogs we search for sources that lie within the 90% uncertainty contour of the alert’s reconstructed direction. For all sources found within the error contour of a given alert, we calculate their angular distance from the best-fit location of the alert. The closest source and its distance from the best-fit location of the alert are reported in Table 3. We find that 139 neutrino alerts have no source from any of the above catalogs in the uncertainty region. For each of the five catalogs, we also determine the total number of alerts that are spatially coincident with at least one source in the catalog. We also determine how many such coincidences are expected due to chance by randomizing the alert directions in right ascension 1000 times and looking at the number of coincidences after each randomization. The sensitivity of IceCube is approximately uniform as a function of right ascension. The randomization allows the production of simulated data with the characteristics of the null hypothesis (no correlation with the catalogs). For each catalog, we find that the number of coincidences is consistent with the median expectation due to chance. The number of observed correlations and the median number expected due to chance for each catalog are shown in Table 2.

³ <https://dataverse.harvard.edu/dataset.xhtml?persistentId=doi:10.7910/DVN/SCRUCD>

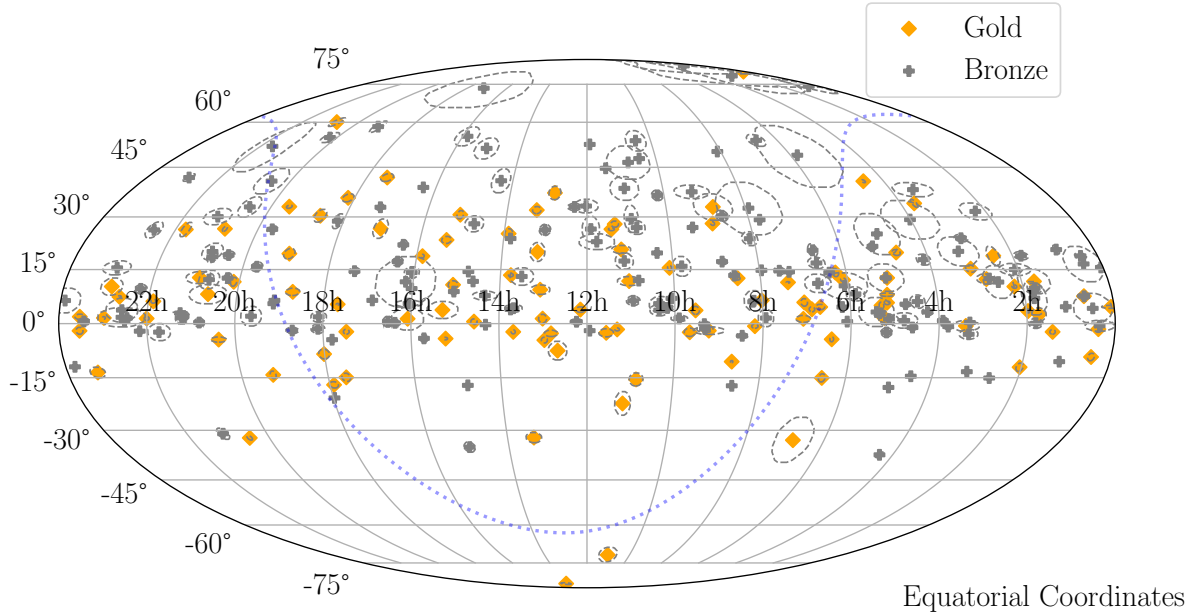


Figure 4. The all-sky distribution of the alerts in the catalog in equatorial coordinates. The orange diamonds show the Gold alerts. The gray crosses show the Bronze alerts. The 90% uncertainty contours at the location of each alert are shown by the dashed ellipses.

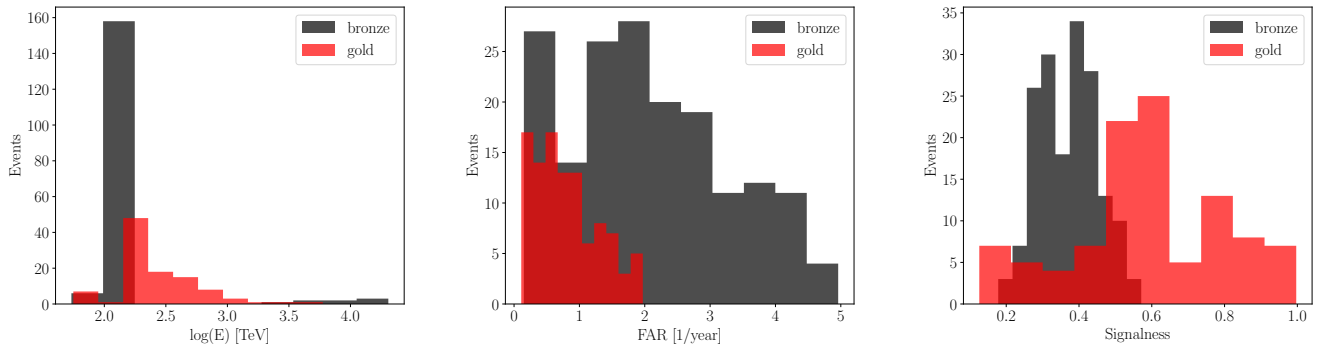


Figure 5. *Left:* The logarithmic distribution of likely neutrino energies (assuming a spectral index of 2.19) in TeV for the catalog. *Center:* The distribution of the false alarm rate of the alerts in the catalog. *Right:* The distribution of signalness of the alerts in the catalog. The red (grey) histogram shows the Gold (Bronze) alerts.

Five Fermi-LAT sources – 4FGL J0914.1-0202, 4FGL J1019.7+0511, 4FGL J2226.6+0210, 4FGL J2227.9+0036 and 4FGL J0244.7+1316 – and one Swift-BAT source, SWIFT J2235.7+013, appear to be spatially correlated with more than one alert, and are considered as repeated candidates for association. The correlations however are not unique as there are often multiple sources located within an error contour. Moreover, such repeated associations are not uncommon in randomized right ascension data sets. For 4FGL alone, we observe on average four candidates for

Table 2. The number of alerts with a particular catalog source located within the error contours, and the number of such observations expected due to chance.

Catalog	Observed Coincidences	Expected Coincidences
4FGL	119	140
3FHL	67	77
3HWC	8	6
TeVCat	12	16
BAT	66	73

repeated associations in 1000 simulations. We emphasize that spatial correlations between neutrino alerts and sources from other catalogs are not evidence for definitive association as the observed number of correlations is consistent with accidental correlations, as shown above. However, we encourage dedicated follow-up studies using the light-curves of the closest sources to each alert identified in this study.

6. SUMMARY AND CONCLUSION

Neutrinos play an extremely important role in the era of multimessenger astronomy, serving as our windows into the complex physics underlying cosmic-ray accelerators. To this end, IceCube has an active program dedicated to immediately alerting the community of a potential astrophysical neutrino detection. The program began in 2016, with significant improvements following in 2019 that are described in this work. Here, we provide a catalog, the IceCube Event Catalog of Alert Tracks (ICECAT-1), of 275 track-like neutrino events that retroactively pass the alert criteria from 2011 to 2020. The event information for each alert is available to the public in the form of FITS (Pence et al. 2010) files that include the complete likelihood profiles providing an accurate grasp on the spatial uncertainty. This catalog, as well as updates with additional alerts, can be found at <https://doi.org/10.7910/DVN/SCRUCD>. This format will also be introduced for future IceCube alerts in addition to the traditional GCN notice format mode of distribution. We have also explored the correlation of IceCube alerts with sources from very-high-energy gamma-ray and X-ray catalogs and find them consistent with chance expectation. Future IceCube analyses, will more systematically explore the correlation of these alerts with blazars, as well as with other IceCube data on long and short time-scales (Abbasi et al. 2021d, 2023). Several observatories have dedicated programs to searching for electromagnetic counterparts of the IceCube real-time alerts leading to the identification of potential sites of cosmic-ray acceleration Necker et al. (2022); Plavin et al. (2020); Dzhappuev et al. (2020); Stein et al. (2021). Multi-wavelength follow-up observations will also benefit from the information provided about IceCube alerts in this catalog. We also note that a revised reconstruction framework is in the works that will improve the angular errors for alerts in the future.

Table 3. Alert events in the catalog along with their time, positions, energy, signalness, and the closest source within the alert error contours from the spatial correlation search. The distance to the coincident sources is shown in parentheses with each source name. Events marked with an asterisk (*) also triggered IceTop and are likely due to cosmic-ray showers. The errors on RA and Dec correspond to the 90% uncertainty likelihood contours (see text).

Alert	MJD	RA [$^{\circ}$]	Dec [$^{\circ}$]	Energy [TeV]	Signalness	Nearest Source ($^{\circ}$)
IC110514A	55695.064	$138.47^{+6.68}_{-3.78}$	$-1.94^{+0.97}_{-1.12}$	187	0.51	4FGL J0914.1-0202 (0.12)
IC110610A	55722.426	$272.55^{+1.67}_{-2.42}$	$35.64^{+1.30}_{-1.05}$	294	0.75	4FGL J1808.8+3522 (0.37)
IC110616A	55728.730	$71.15^{+1.41}_{-2.07}$	$5.38^{+0.79}_{-0.90}$	109	0.26	... (...)

Table 3 continued on next page

Table 3 (continued)

Alert	MJD	RA [°]	Dec [°]	Energy [TeV]	Signalness	Nearest Source (°)
IC110714A	55756.113	68.20 ^{+0.31} _{-1.10}	40.67 ^{+0.44} _{-0.44}	72	0.78	... (...)
IC110726A	55768.511	151.08 ^{+1.19} _{-1.71}	6.99 ^{+0.98} _{-0.83}	160	0.40	... (...)
IC110807A	55780.980	336.80 ^{+1.36} _{-1.98}	1.53 ^{+0.93} _{-0.78}	108	0.27	4FGL J2226.6+0210 (0.65)
IC110818A	55791.689	332.45 ^{+0.97} _{-1.23}	-2.09 ^{+0.93} _{-0.90}	123	0.34	... (...)
IC110902A	55806.092	9.76 ^{+2.86} _{-1.32}	7.59 ^{+0.87} _{-0.86}	243	0.61	... (...)
IC110907A	55811.795	196.08 ^{+3.91} _{-2.68}	9.40 ^{+1.55} _{-1.06}	186	0.51	4FGL J1301.6+0834 (1.06)
IC110929A	55833.260	121.45 ^{+1.34} _{-1.29}	50.04 ^{+0.24} _{-0.15}	158	0.52	... (...)
IC110930A	55834.445	267.01 ^{+1.19} _{-1.14}	-4.44 ^{+0.60} _{-0.79}	160	0.43	... (...)
IC111012A	55846.867	172.13 ^{+1.40} _{-1.39}	44.70 ^{+0.79} _{-0.45}	115	0.43	... (...)
IC111120A	55885.961	26.06 ^{+1.89} _{-3.16}	9.82 ^{+1.40} _{-1.36}	159	0.42	... (...)
IC111120B*	55885.973	356.84 ^{+0.53} _{-0.62}	-11.99 ^{+0.23} _{-0.27}	4969	0.29	... (...)
IC111208A	55903.719	165.19 ^{+7.03} _{-4.13}	38.49 ^{+3.67} _{-3.49}	123	0.45	4FGL J1101.5+3904 (0.6)
IC111209A	55904.457	99.98 ^{+1.19} _{-2.02}	20.42 ^{+1.60} _{-2.02}	108	0.34	3HWC J0633+191 (1.95)
IC111213A	55908.398	247.85 ^{+1.71} _{-1.58}	0.56 ^{+1.46} _{-1.42}	164	0.41	4FGL J1638.0+0042 (1.67)
IC111216A	55911.277	36.74 ^{+1.80} _{-2.24}	18.88 ^{+2.46} _{-2.82}	891	0.95	SWIFT J0225.0+18 (0.46)
IC111218A	55913.335	26.85 ^{+3.69} _{-4.66}	7.03 ^{+4.04} _{-5.20}	157	0.40	3FHL J0151.0+0539 (1.64)
IC120301A	55987.807	237.96 ^{+0.53} _{-0.62}	18.76 ^{+0.47} _{-0.51}	433	0.82	... (...)
IC120426A	56043.415	183.56 ^{+2.15} _{-2.02}	0.52 ^{+0.86} _{-0.71}	109	0.27	... (...)
IC120501A	56048.570	165.37 ^{+7.01} _{-5.36}	-71.51 ^{+3.53} _{-2.68}	85	0.46	... (...)
IC120515A	56062.959	198.94 ^{+1.71} _{-1.41}	32.00 ^{+0.97} _{-1.09}	194	0.61	... (...)
IC120523A	56070.574	171.08 ^{+0.66} _{-1.41}	26.44 ^{+0.46} _{-0.37}	213	0.53	... (...)
IC120523A	56070.639	343.78 ^{+4.92} _{-4.48}	15.48 ^{+2.38} _{-1.54}	168	0.49	4FGL J2253.9+1609 (0.72)
IC120529A	56076.543	176.48 ^{+6.64} _{-5.93}	22.87 ^{+2.70} _{-1.77}	126	0.42	SWIFT J1141.3+21 (1.45)
IC120601A	56079.306	119.31 ^{+2.02} _{-0.92}	14.79 ^{+0.62} _{-0.73}	137	0.40	... (...)
IC120605A	56083.655	152.58 ^{+1.89} _{-2.42}	36.38 ^{+1.54} _{-1.47}	107	0.39	4FGL J1011.6+3600 (0.45)
IC120611A*	56089.364	39.95 ^{+0.26} _{-0.26}	-15.09 ^{+0.19} _{-0.31}	9220	0.24	... (...)
IC120807A	56146.207	330.07 ^{+0.83} _{-0.83}	1.42 ^{+0.60} _{-0.45}	373	0.74	... (...)
IC120916A	56186.305	182.24 ^{+1.36} _{-1.71}	3.88 ^{+0.67} _{-0.82}	174	0.44	4FGL J1204.8+0407 (1.06)
IC120922A	56192.549	70.62 ^{+1.49} _{-1.27}	19.79 ^{+0.91} _{-0.71}	143	0.43	... (...)
IC121011A	56211.771	205.14 ^{+0.66} _{-0.70}	-2.28 ^{+0.52} _{-0.56}	481	0.84	... (...)
IC121026A	56226.599	169.80 ^{+1.32} _{-1.41}	27.91 ^{+0.85} _{-0.88}	961	0.93	... (...)
IC121103A	56234.508	123.18 ^{+0.92} _{-0.97}	6.05 ^{+0.64} _{-0.56}	112	0.28	... (...)
IC121115A	56246.330	225.70 ^{+1.01} _{-1.19}	8.88 ^{+0.94} _{-0.95}	116	0.32	... (...)
IC130125A	56317.266	7.67 ^{+6.46} _{-5.92}	74.14 ^{+3.36} _{-2.82}	165	0.53	4FGL J0028.1+7505 (0.97)
IC130125A	56317.659	280.46 ^{+1.89} _{-2.33}	-1.90 ^{+0.93} _{-0.82}	114	0.31	4FGL J1847.2-0141 (1.37)
IC130127A	56319.280	352.97 ^{+1.32} _{-1.01}	-1.98 ^{+0.97} _{-0.90}	235	0.61	4FGL J2333.4-0133 (0.58)
IC130208A*	56331.121	48.38 ^{+0.31} _{-0.31}	-13.32 ^{+0.23} _{-0.23}	2268	0.32	... (...)
IC130316A	56367.736	303.41 ^{+2.98} _{-3.55}	54.68 ^{+1.77} _{-1.59}	105	0.38	SWIFT J2006.5+56 (1.93)
IC130318A	56369.285	13.45 ^{+0.79} _{-0.88}	20.62 ^{+1.44} _{-0.99}	106	0.33	... (...)
IC130408A	56390.189	167.83 ^{+2.64} _{-3.96}	20.66 ^{+1.28} _{-0.99}	65	0.53	SWIFT J1114.3+20 (0.71)

Table 3 continued on next page

Table 3 (continued)

Alert	MJD	RA [°]	Dec [°]	Energy [TeV]	Signalness	Nearest Source (°)
IC130408B	56390.758	$7.38^{+4.88}_{-8.04}$	$4.22^{+4.73}_{-3.58}$	163	0.40	4FGL J0030.4+0451 (0.68)
IC130409A	56391.982	$163.56^{+2.68}_{-2.50}$	$29.44^{+4.38}_{-3.46}$	115	0.41	GB6 J1058+2817 (1.48)
IC130508A	56420.641	$337.76^{+3.21}_{-2.02}$	$26.24^{+2.69}_{-1.90}$	140	0.45	SWIFT J2237.0+25 (1.35)
IC130509A	56421.186	$317.50^{+1.76}_{-1.85}$	$2.09^{+1.19}_{-1.34}$	105	0.25	4FGL J2104.7+0108 (1.63)
IC130519A	56431.483	$45.35^{+3.12}_{-1.49}$	$23.85^{+1.15}_{-0.89}$	110	0.36	... (...)
IC130531A	56443.557	$164.18^{+2.42}_{-2.15}$	$6.32^{+1.32}_{-1.27}$	143	0.35	... (...)
IC130627A	56470.110	$93.74^{+1.01}_{-1.14}$	$14.17^{+1.23}_{-1.04}$	851	0.94	4FGL J0615.9+1416 (0.26)
IC130627B	56470.426	$155.35^{+3.87}_{-2.37}$	$3.73^{+1.72}_{-1.42}$	122	0.31	... (...)
IC130711A	56484.530	$77.87^{+2.59}_{-1.19}$	$-2.43^{+1.34}_{-1.12}$	165	0.43	4FGL J0515.5-0125 (1.44)
IC130731A	56504.072	$122.87^{+2.29}_{-4.35}$	$6.32^{+3.24}_{-2.40}$	122	0.32	4FGL J0812.5+0711 (0.92)
IC130801A	56505.256	$214.98^{+4.35}_{-4.00}$	$7.75^{+1.24}_{-1.20}$	110	0.28	SWIFT J1419.1+07 (0.26)
IC130804A	56508.815	$129.02^{+1.14}_{-1.54}$	$13.36^{+1.08}_{-1.68}$	113	0.33	... (...)
IC130808A	56512.340	$26.59^{+1.14}_{-1.23}$	$9.22^{+0.91}_{-0.87}$	111	0.29	... (...)
IC130822A	56526.409	$91.32^{+1.19}_{-1.19}$	$0.56^{+0.78}_{-0.63}$	115	0.30	3FHL J0604.9+0000 (0.56)
IC130907A*	56542.793	$130.17^{+0.48}_{-0.31}$	$-10.54^{+0.27}_{-0.30}$	890	0.32	... (...)
IC131014A	56579.909	$32.92^{+0.88}_{-0.70}$	$10.28^{+0.42}_{-0.57}$	293	0.67	... (...)
IC131023A	56588.559	$301.90^{+1.01}_{-1.05}$	$11.61^{+1.14}_{-1.29}$	211	0.59	... (...)
IC131108A	56604.553	$342.73^{+1.54}_{-1.58}$	$41.81^{+1.40}_{-0.89}$	153	0.50	... (...)
IC131112A	56608.031	$129.24^{+0.26}_{-0.26}$	$-17.27^{+0.16}_{-0.16}$	7006	0.27	... (...)
IC131124A	56620.145	$285.16^{+2.20}_{-1.54}$	$19.47^{+1.43}_{-1.46}$	180	0.55	... (...)
IC131204A	56630.470	$288.98^{+1.10}_{-0.83}$	$-14.21^{+0.77}_{-1.31}$	259	0.20	4FGL J1916.7-1516 (1.08)
IC140101A	56658.404	$192.26^{+2.07}_{-2.37}$	$-2.69^{+1.01}_{-0.71}$	200	0.56	4FGL J1251.3-0201 (0.88)
IC140103A	56660.886	$37.90^{+25.61}_{-27.30}$	$78.97^{+5.86}_{-9.97}$	125	0.42	4FGL J0226.9+7744 (1.25)
IC140108A	56665.308	$344.66^{+0.53}_{-0.48}$	$1.57^{+0.37}_{-0.34}$	214	0.69	... (...)
IC140109A	56666.503	$293.12^{+0.79}_{-1.19}$	$33.02^{+0.45}_{-0.53}$	924	0.93	SWIFT J1933.9+32 (0.31)
IC140114A	56671.878	$337.59^{+0.57}_{-0.92}$	$0.71^{+0.97}_{-0.86}$	54	0.34	4FGL J2227.9+0036 (0.61)
IC140122A	56679.147	$138.82^{+3.52}_{-10.11}$	$37.45^{+1.95}_{-2.09}$	131	0.46	SWIFT J0920.1+37 (0.99)
IC140122B	56679.204	$220.29^{+8.94}_{-8.37}$	$-86.07^{+0.59}_{-0.64}$	374	0.82	... (...)
IC140203A	56691.785	$349.58^{+2.64}_{-2.55}$	$-13.55^{+1.15}_{-1.73}$	685	0.13	... (...)
IC140213A	56701.809	$202.59^{+4.79}_{-3.21}$	$13.06^{+2.31}_{-2.52}$	140	0.39	4FGL J1326.1+1232 (1.14)
IC140223A	56711.920	$118.83^{+11.87}_{-11.87}$	$32.58^{+5.68}_{-9.83}$	119	0.43	4FGL J0752.2+3313 (0.92)
IC140307A	56723.920	$308.06^{+2.68}_{-4.61}$	$32.93^{+2.71}_{-3.23}$	109	0.40	4FGL J2028.3+3331 (1.01)
IC140324A	56740.089	$225.70^{+5.67}_{-4.65}$	$51.06^{+4.00}_{-2.87}$	109	0.40	4FGL J1456.0+5051 (1.08)
IC140410A	56757.099	$2.11^{+151.51}_{-58.92}$	$81.22^{+8.00}_{-6.94}$	246	0.63	SWIFT J0017.1+81 (0.5)
IC140411A	56758.567	$146.95^{+3.12}_{-3.12}$	$15.91^{+2.89}_{-2.62}$	156	0.45	4FGL J0949.2+1749 (1.95)
IC140420A	56767.859	$6.28^{+7.03}_{-5.89}$	$16.57^{+4.77}_{-5.11}$	163	0.49	4FGL J0023.9+1603 (0.58)
IC140503A	56780.957	$162.30^{+6.91}_{-11.26}$	$46.57^{+5.41}_{-5.11}$	109	0.40	3FHL J1053.6+4930 (3.03)
IC140603A	56811.142	$9.71^{+0.62}_{-0.88}$	$7.56^{+0.53}_{-0.83}$	152	0.38	... (...)
IC140609A	56817.636	$106.26^{+2.68}_{-2.15}$	$1.31^{+1.05}_{-0.86}$	459	0.81	... (...)
IC140611A	56819.204	$110.65^{+0.53}_{-0.62}$	$11.45^{+0.19}_{-0.19}$	5960	1.00	... (...)

Table 3 continued on next page

Table 3 (continued)

Alert	MJD	RA [°]	Dec [°]	Energy [TeV]	Signalness	Nearest Source (°)
IC140704A	56842.298	157.07 ^{+4.69} _{-4.64}	53.62 ^{+3.35} _{-3.48}	150	0.50	SWIFT J1033.8+52 (1.07)
IC140705A	56843.669	25.88 ^{+1.85} _{-2.99}	2.54 ^{+1.79} _{-1.75}	212	0.56	4FGL J0138.5+0300 (1.33)
IC140707A	56845.500	240.86 ^{+3.08} _{-2.07}	14.17 ^{+1.54} _{-1.65}	167	0.48	4FGL J1606.2+1346 (0.8)
IC140713A	56851.557	0.79 ^{+1.14} _{-1.19}	15.60 ^{+0.89} _{-0.66}	134	0.39	... (...)
IC140721A	56859.759	101.82 ^{+6.77} _{-6.86}	-32.89 ^{+5.23} _{-8.08}	157	0.56	4FGL J0649.5-3139 (1.32)
IC140820A	56889.378	271.45 ^{+3.43} _{-1.80}	1.87 ^{+1.42} _{-1.46}	108	0.27	... (...)
IC140923A	56923.721	169.72 ^{+0.70} _{-0.83}	-1.60 ^{+0.52} _{-0.30}	209	0.24	... (...)
IC140927A	56927.161	50.89 ^{+3.91} _{-5.14}	-0.63 ^{+1.49} _{-1.42}	182	0.48	3FHL J0323.6-0109 (0.54)
IC141012A	56942.751	63.85 ^{+2.24} _{-1.36}	3.21 ^{+0.90} _{-1.08}	173	0.44	4FGL J0412.3+0239 (0.94)
IC141110A	56971.297	253.43 ^{+0.83} _{-1.10}	6.43 ^{+0.71} _{-0.68}	113	0.29	... (...)
IC141114A	56975.257	221.48 ^{+4.53} _{-2.29}	28.00 ^{+2.31} _{-2.30}	110	0.38	3FHL J1449.5+2745 (0.84)
IC141208A	56999.668	246.36 ^{+1.76} _{-1.89}	17.23 ^{+1.29} _{-1.09}	109	0.33	4FGL J1626.4+1820 (1.13)
IC141210A	57001.848	318.12 ^{+2.33} _{-1.93}	1.57 ^{+1.57} _{-1.72}	154	0.37	... (...)
IC141221A	57012.410	179.08 ^{+0.88} _{-1.10}	-1.94 ^{+0.71} _{-0.82}	134	0.35	... (...)
IC150102A	57024.796	318.74 ^{+3.96} _{-1.27}	2.91 ^{+0.34} _{-0.49}	126	0.32	... (...)
IC150104A	57026.399	272.11 ^{+1.71} _{-1.54}	28.76 ^{+2.41} _{-1.86}	133	0.45	4FGL J1807.1+2822 (0.48)
IC150118A	57040.509	152.53 ^{+1.54} _{-2.72}	4.33 ^{+0.71} _{-0.86}	156	0.37	... (...)
IC150119A	57041.369	286.92 ^{+1.36} _{-1.27}	6.43 ^{+0.60} _{-0.53}	140	0.35	3HWC J1908+063 (0.14)
IC150120A	57042.985	95.89 ^{+1.19} _{-1.36}	14.13 ^{+0.50} _{-0.50}	113	0.34	... (...)
IC150127A	57049.481	100.37 ^{+1.36} _{-1.63}	4.59 ^{+0.79} _{-0.67}	293	0.66	... (...)
IC150129A	57051.227	358.51 ^{+3.91} _{-6.55}	6.39 ^{+3.16} _{-3.67}	130	0.33	4FGL J2349.4+0534 (1.41)
IC150224A	57078.000	237.75 ^{+8.26} _{-2.26}	55.11 ^{+3.38} _{-3.03}	106	0.38	4FGL J1553.1+5438 (0.56)
IC150313A	57094.321	127.05 ^{+1.76} _{-2.07}	-3.36 ^{+0.75} _{-0.75}	107	0.29	... (...)
IC150428A	57140.591	31.07 ^{+4.04} _{-6.42}	15.02 ^{+1.94} _{-1.42}	109	0.32	4FGL J0204.8+1513 (0.26)
IC150515A	57157.942	91.49 ^{+0.92} _{-0.75}	12.14 ^{+0.53} _{-0.50}	401	0.77	... (...)
IC150526A	57168.017	139.79 ^{+2.46} _{-2.99}	-1.49 ^{+0.90} _{-1.01}	108	0.28	4FGL J0914.1-0202 (1.36)
IC150601A	57174.018	333.37 ^{+2.42} _{-1.71}	9.63 ^{+1.21} _{-1.17}	106	0.27	... (...)
IC150609A	57182.027	49.53 ^{+1.10} _{-1.10}	0.30 ^{+0.45} _{-0.82}	118	0.31	... (...)
IC150609B	57182.180	245.43 ^{+1.67} _{-1.23}	0.22 ^{+1.04} _{-0.93}	116	0.30	4FGL J1625.1-0020 (1.03)
IC150625A	57198.640	71.89 ^{+4.35} _{-4.70}	0.86 ^{+2.39} _{-1.83}	112	0.29	4FGL J0442.6-0017 (1.69)
IC150625B	57198.732	306.43 ^{+2.02} _{-2.02}	19.08 ^{+0.91} _{-1.18}	154	0.46	4FGL J2030.9+1935 (1.34)
IC150714A	57217.910	326.29 ^{+1.49} _{-1.32}	26.36 ^{+1.89} _{-2.19}	439	0.84	... (...)
IC150809A*	57243.322	221.75 ^{+0.31} _{-0.26}	-17.15 ^{+0.23} _{-0.16}	11667	0.20	... (...)
IC150812A	57246.318	317.59 ^{+5.10} _{-4.66}	30.09 ^{+2.31} _{-2.43}	125	0.44	3FHL J2115.2+2933 (1.19)
IC150812B	57246.759	328.27 ^{+0.75} _{-0.88}	6.17 ^{+0.49} _{-0.53}	508	0.83	... (...)
IC150823A	57257.623	325.90 ^{+3.47} _{-4.17}	-2.35 ^{+2.61} _{-2.09}	133	0.35	4FGL J2148.9-0121 (1.66)
IC150831A	57265.218	54.76 ^{+0.92} _{-0.92}	34.00 ^{+1.13} _{-1.21}	181	0.58	... (...)
IC150904A	57269.760	133.77 ^{+0.53} _{-0.88}	28.08 ^{+0.51} _{-0.55}	302	0.74	3FHL J0854.1+2752 (0.29)
IC150914A	57279.875	129.68 ^{+1.89} _{-2.59}	30.35 ^{+1.88} _{-1.29}	120	0.43	SWIFT J0840.2+29 (0.63)
IC150918A	57283.546	49.83 ^{+2.50} _{-3.74}	-2.95 ^{+1.35} _{-1.34}	105	0.28	SWIFT J0324.9-03 (1.41)

Table 3 continued on next page

Table 3 (continued)

Alert	MJD	RA	Dec	Energy	Signalness	Nearest Source (°)
		[°]	[°]	[TeV]		
IC150919A	57284.206	279.54 ^{+1.76} _{-2.29}	30.35 ^{+2.19} _{-1.50}	228	0.67	4FGL J1836.4+3137 (1.32)
IC150923A	57288.027	103.23 ^{+0.70} _{-1.14}	3.96 ^{+0.60} _{-0.75}	216	0.33	... (...)
IC150926A	57291.901	194.55 ^{+0.79} _{-1.23}	-4.56 ^{+0.93} _{-0.64}	216	0.30	4FGL J1258.7-0452 (0.34)
IC151013A	57308.124	178.72 ^{+1.11} _{-1.15}	52.37 ^{+1.11} _{-1.11}	156	0.52	... (...)
IC151017A	57312.676	197.53 ^{+2.46} _{-2.72}	19.95 ^{+3.01} _{-2.29}	321	0.75	4FGL J1311.8+2057 (1.09)
IC151114A	57340.873	76.16 ^{+1.36} _{-1.36}	12.71 ^{+0.65} _{-0.73}	1124	0.96	... (...)
IC151122A	57348.532	262.05 ^{+0.88} _{-1.05}	-2.24 ^{+0.63} _{-0.67}	253	0.64	... (...)
IC160104A	57391.444	79.41 ^{+0.83} _{-0.75}	5.00 ^{+0.86} _{-0.97}	217	0.57	4FGL J0515.9+0537 (0.75)
IC160128A	57415.183	263.76 ^{+1.10} _{-1.80}	-14.90 ^{+1.08} _{-1.20}	583	0.15	... (...)
IC160225A	57443.880	311.87 ^{+2.18} _{-1.78}	60.06 ^{+1.65} _{-1.37}	188	0.60	... (...)
IC160307A	57454.697	91.32 ^{+7.08} _{-8.66}	10.47 ^{+2.74} _{-4.45}	106	0.28	4FGL J0608.6+1149 (1.59)
IC160331A	57478.565	151.22 ^{+0.66} _{-0.66}	15.48 ^{+0.66} _{-0.73}	492	0.85	... (...)
IC160410A	57488.735	235.63 ^{+1.23} _{-1.45}	-4.07 ^{+1.31} _{-0.86}	131	0.37	... (...)
IC160427A	57505.245	240.29 ^{+0.44} _{-0.48}	9.71 ^{+0.57} _{-0.42}	85	0.45	... (...)
IC160510A	57518.664	352.88 ^{+1.76} _{-1.45}	1.90 ^{+0.75} _{-0.67}	208	0.39	... (...)
IC160612A	57551.434	16.52 ^{+0.88} _{-0.18}	4.67 ^{+1.87} _{-0.52}	106	0.25	... (...)
IC160614A	57553.526	214.76 ^{+3.16} _{-4.13}	40.82 ^{+3.33} _{-3.98}	112	0.41	4FGL J1421.1+3859 (1.87)
IC160615A	57554.404	304.32 ^{+1.63} _{-1.05}	12.64 ^{+1.33} _{-1.34}	150	0.41	4FGL J2014.9+1225 (0.61)
IC160707A	57576.168	351.43 ^{+1.54} _{-2.29}	0.60 ^{+0.82} _{-1.12}	110	0.28	4FGL J2326.2+0113 (0.64)
IC160720A	57589.914	60.25 ^{+10.72} _{-8.88}	29.23 ^{+5.32} _{-5.87}	108	0.37	4FGL J0358.1+2850 (0.74)
IC160727A	57596.344	113.12 ^{+1.93} _{-1.54}	14.67 ^{+1.08} _{-1.12}	105	0.30	... (...)
IC160731A	57600.080	214.58 ^{+0.53} _{-0.57}	-0.30 ^{+0.45} _{-0.67}	98	0.44	... (...)
IC160731A	57600.785	312.63 ^{+3.74} _{-3.21}	20.07 ^{+2.56} _{-2.13}	118	0.39	4FGL J2043.9+2051 (1.73)
IC160806A	57606.515	122.78 ^{+0.88} _{-1.23}	-0.71 ^{+0.56} _{-0.56}	219	0.58	... (...)
IC160812A	57612.684	86.99 ^{+15.29} _{-15.29}	48.83 ^{+9.95} _{-10.00}	160	0.53	4FGL J0553.5+4810 (1.14)
IC160814A	57614.907	200.04 ^{+3.12} _{-2.68}	-32.13 ^{+1.75} _{-1.24}	263	0.61	SWIFT J1325.2-32 (1.25)
IC160924A	57655.741	241.13 ^{+4.92} _{-5.89}	1.34 ^{+3.40} _{-2.80}	191	0.51	4FGL J1608.4+0055 (1.07)
IC161001A	57662.439	192.57 ^{+2.50} _{-2.07}	37.12 ^{+1.51} _{-2.49}	204	0.64	4FGL J1249.8+3707 (0.09)
IC161012A	57673.613	190.06 ^{+2.20} _{-4.04}	-7.48 ^{+2.18} _{-2.98}	759	0.25	SWIFT J1239.6-05 (2.14)
IC161021A	57682.309	121.42 ^{+2.64} _{-2.90}	23.72 ^{+1.93} _{-2.02}	135	0.43	4FGL J0803.0+2439 (1.12)
IC161027A	57688.570	119.00 ^{+2.94} _{-2.24}	1.53 ^{+2.32} _{-2.39}	155	0.38	... (...)
IC161103A	57695.380	40.87 ^{+1.05} _{-0.57}	12.52 ^{+1.15} _{-0.61}	85	0.31	4FGL J0244.7+1316 (0.82)
IC161117A	57709.332	78.66 ^{+1.85} _{-1.93}	1.60 ^{+1.90} _{-1.79}	190	0.50	... (...)
IC161125A	57717.430	140.01 ^{+2.15} _{-1.19}	-0.11 ^{+0.75} _{-0.86}	161	0.40	... (...)
IC161127A	57719.665	257.55 ^{+36.46} _{-29.23}	73.27 ^{+5.71} _{-9.96}	139	0.45	4FGL J1651.6+7219 (1.66)
IC161210A	57732.838	46.36 ^{+2.37} _{-0.92}	15.25 ^{+0.93} _{-1.08}	80	0.38	... (...)
IC161224A	57746.537	61.79 ^{+2.50} _{-2.37}	17.78 ^{+1.46} _{-1.56}	139	0.42	SWIFT J0413.3+16 (1.69)
IC170105A	57758.142	309.95 ^{+5.01} _{-7.56}	8.16 ^{+2.00} _{-3.34}	198	0.54	SWIFT J2033.1+09 (2.41)
IC170206A	57790.549	180.35 ^{+5.23} _{-3.82}	33.20 ^{+1.85} _{-2.16}	135	0.46	4FGL J1205.8+3321 (0.94)
IC170208A	57792.128	99.67 ^{+2.59} _{-3.30}	16.84 ^{+1.60} _{-1.55}	151	0.43	3HWC J0634+165 (1.14)

Table 3 continued on next page

Table 3 (continued)

Alert	MJD	RA [°]	Dec [°]	Energy [TeV]	Signalness	Nearest Source (°)
IC170208A	57792.595	92.81 ^{+1.23} _{-1.05}	4.59 ^{+0.94} _{-1.16}	133	0.33	... (...)
IC170227A	57811.065	205.09 ^{+1.89} _{-3.96}	4.26 ^{+1.09} _{-1.12}	108	0.27	SWIFT J1338.2+04 (0.59)
IC170308A	57820.925	155.35 ^{+2.02} _{-1.19}	5.53 ^{+0.98} _{-0.90}	107	0.25	4FGL J1019.7+0511 (0.53)
IC170321A	57833.314	98.26 ^{+1.32} _{-0.92}	-15.06 ^{+1.04} _{-1.20}	231	0.24	... (...)
IC170422A	57865.646	240.95 ^{+3.34} _{-5.71}	5.53 ^{+0.83} _{-1.01}	161	0.39	... (...)
IC170427A	57870.314	5.32 ^{+4.48} _{-5.27}	-0.60 ^{+1.75} _{-1.23}	155	0.38	3FHL J0022.0+0006 (0.73)
IC170514A	57887.175	311.97 ^{+2.20} _{-1.23}	18.60 ^{+2.10} _{-1.10}	109	0.34	... (...)
IC170514B	57887.300	227.37 ^{+1.23} _{-1.10}	30.65 ^{+1.40} _{-0.99}	174	0.55	... (...)
IC170527A	57900.070	178.59 ^{+2.77} _{-3.47}	26.49 ^{+3.82} _{-3.45}	124	0.42	4FGL J1148.5+2629 (1.3)
IC170621A	57925.191	74.97 ^{+7.25} _{-7.78}	25.08 ^{+5.57} _{-6.20}	109	0.37	SWIFT J0502.4+24 (0.68)
IC170626A	57930.519	280.99 ^{+3.03} _{-1.63}	8.80 ^{+1.13} _{-0.90}	201	0.55	4FGL J1846.3+0919 (0.8)
IC170704A	57938.293	230.45 ^{+1.67} _{-1.71}	23.36 ^{+1.10} _{-0.89}	195	0.60	... (...)
IC170717A	57951.818	208.39 ^{+1.67} _{-1.19}	25.16 ^{+1.41} _{-1.35}	534	0.87	... (...)
IC170803A	57968.084	1.10 ^{+4.48} _{-1.76}	4.63 ^{+0.41} _{-0.41}	214	0.56	... (...)
IC170809A	57974.597	21.27 ^{+0.75} _{-1.05}	-2.28 ^{+0.60} _{-0.67}	226	0.60	... (...)
IC170819A	57984.276	26.98 ^{+1.85} _{-3.03}	18.88 ^{+1.11} _{-1.10}	167	0.51	... (...)
IC170824A	57989.554	41.92 ^{+3.03} _{-3.56}	12.37 ^{+1.46} _{-1.30}	175	0.49	SWIFT J0248.3+12 (0.38)
IC170922A	58018.871	77.43 ^{+1.14} _{-0.75}	5.79 ^{+0.64} _{-0.41}	264	0.63	3FHL J0509.4+0542 (0.11)
IC170923A	58019.021	173.45 ^{+2.37} _{-2.55}	-2.54 ^{+0.90} _{-1.31}	202	0.56	... (...)
IC171006A	58032.308	132.63 ^{+1.41} _{-2.24}	17.23 ^{+1.06} _{-0.66}	118	0.37	... (...)
IC171015A	58041.066	162.91 ^{+2.99} _{-1.71}	-15.48 ^{+1.62} _{-1.98}	72	0.55	SWIFT J1051.2-170 (1.58)
IC171028A	58054.765	294.52 ^{+3.56} _{-3.38}	2.05 ^{+2.20} _{-3.21}	133	0.34	3FHL J1927.5+0153 (2.64)
IC171106A	58063.778	340.14 ^{+0.62} _{-0.62}	7.44 ^{+0.30} _{-0.26}	1573	0.97	... (...)
IC171108A*	58065.755	269.65 ^{+0.22} _{-0.18}	-20.70 ^{+0.16} _{-0.16}	20310	0.18	... (...)
IC180117A	58135.752	206.10 ^{+1.19} _{-1.14}	3.92 ^{+0.71} _{-0.78}	85	0.42	... (...)
IC180123A	58141.677	77.12 ^{+2.50} _{-2.90}	8.01 ^{+0.41} _{-0.49}	416	0.79	... (...)
IC180125A	58143.976	207.51 ^{+1.01} _{-0.57}	23.77 ^{+0.57} _{-0.57}	110	0.36	... (...)
IC180205A	58154.004	17.40 ^{+1.36} _{-0.92}	-10.54 ^{+0.76} _{-0.72}	113	0.23	... (...)
IC180213A	58162.378	66.97 ^{+2.46} _{-2.59}	6.09 ^{+1.95} _{-1.72}	111	0.27	4FGL J0427.3+0504 (1.02)
IC180228A	58177.572	294.79 ^{+1.85} _{-1.71}	26.40 ^{+0.79} _{-1.12}	124	0.42	... (...)
IC180313A	58190.679	287.18 ^{+0.75} _{-2.46}	5.53 ^{+0.34} _{-0.26}	160	0.39	... (...)
IC180314A	58191.804	58.71 ^{+1.89} _{-1.67}	0.78 ^{+1.01} _{-1.01}	145	0.36	... (...)
IC180316A	58193.243	271.71 ^{+1.19} _{-3.43}	-1.42 ^{+1.23} _{-1.27}	156	0.39	4FGL J1759.0-0107 (1.97)
IC180410A	58218.777	218.50 ^{+0.79} _{-1.27}	0.56 ^{+0.75} _{-0.71}	234	0.60	... (...)
IC180417A	58225.279	305.73 ^{+3.60} _{-1.58}	-4.41 ^{+0.67} _{-0.75}	202	0.58	... (...)
IC180528A	58266.506	312.14 ^{+1.41} _{-2.02}	0.30 ^{+0.86} _{-1.45}	110	0.28	4FGL J2049.7-0036 (0.97)
IC180608A	58277.597	69.08 ^{+1.63} _{-1.41}	-1.08 ^{+0.78} _{-0.78}	158	0.40	4FGL J0436.2-0038 (0.43)
IC180612A	58281.190	338.69 ^{+5.10} _{-5.71}	3.73 ^{+2.81} _{-3.70}	107	0.25	SWIFT J2235.7+01 (2.12)
IC180613A	58282.982	38.06 ^{+5.84} _{-4.26}	11.53 ^{+4.15} _{-4.91}	155	0.41	4FGL J0231.8+1322 (1.84)
IC180728A*	58327.845	74.14 ^{+0.44} _{-0.35}	-17.74 ^{+0.51} _{-0.59}	16952	0.18	... (...)

Table 3 continued on next page

Table 3 (continued)

Alert	MJD	RA [°]	Dec [°]	Energy [TeV]	Signalness	Nearest Source (°)
IC180807A	58337.202	100.37 ^{+4.00} _{-5.05}	11.15 ^{+2.98} _{-2.12}	106	0.28	4FGL J0642.4+1048 (0.41)
IC180908A	58369.833	144.98 ^{+1.49} _{-2.20}	-2.39 ^{+1.16} _{-1.12}	144	0.30	... (...)
IC180909A	58370.604	141.37 ^{+1.05} _{-1.27}	26.94 ^{+0.88} _{-1.00}	171	0.53	... (...)
IC180919A	58380.065	258.40 ^{+1.49} _{-1.49}	32.84 ^{+0.94} _{-0.75}	144	0.48	4FGL J1714.6+3228 (0.43)
IC181008A	58399.779	77.08 ^{+2.68} _{-3.56}	1.23 ^{+1.23} _{-1.16}	108	0.27	... (...)
IC181014A	58405.495	225.22 ^{+1.36} _{-2.64}	-34.95 ^{+1.22} _{-1.79}	62	0.39	4FGL J1505.0-3433 (0.94)
IC181023A	58414.693	270.18 ^{+1.89} _{-1.71}	-8.42 ^{+1.13} _{-1.55}	237	0.15	4FGL J1804.4-0852 (1.03)
IC181023B	58414.736	78.27 ^{+1.76} _{-0.92}	21.54 ^{+0.96} _{-0.93}	136	0.43	... (...)
IC181114A	58436.945	6.02 ^{+1.63} _{-2.24}	18.84 ^{+0.87} _{-0.98}	145	0.44	... (...)
IC181120A	58442.709	25.71 ^{+5.54} _{-5.27}	11.72 ^{+2.41} _{-4.50}	188	0.54	4FGL J0150.9+1230 (2.13)
IC181120B	58442.944	324.58 ^{+7.74} _{-9.04}	51.74 ^{+6.75} _{-9.48}	173	0.57	SWIFT J2133.6+51 (0.94)
IC181121A	58443.580	132.19 ^{+7.34} _{-6.99}	32.93 ^{+4.19} _{-3.57}	209	0.65	SWIFT J0848.1+34 (1.81)
IC181212A	58464.085	316.41 ^{+1.85} _{-2.02}	-31.00 ^{+1.68} _{-1.58}	162	0.46	4FGL J2112.5-3043 (1.51)
IC190113A	58496.089	56.91 ^{+1.63} _{-1.41}	-0.82 ^{+0.75} _{-0.82}	156	0.39	... (...)
IC190124A	58507.155	307.44 ^{+0.53} _{-1.14}	-32.22 ^{+0.96} _{-0.31}	157	0.74	... (...)
IC190201A	58515.016	245.08 ^{+0.75} _{-0.88}	38.78 ^{+0.77} _{-0.67}	163	0.53	... (...)
IC190214A	58528.673	228.25 ^{+0.79} _{-0.53}	-4.14 ^{+0.37} _{-0.30}	348	0.74	... (...)
IC190221A	58535.351	268.59 ^{+1.41} _{-1.58}	-17.00 ^{+1.24} _{-0.51}	56	0.55	... (...)
IC190223A	58537.850	155.21 ^{+0.70} _{-0.66}	19.67 ^{+0.28} _{-0.44}	168	0.51	... (...)
IC190317A	58559.832	81.25 ^{+5.89} _{-5.98}	3.21 ^{+3.93} _{-4.07}	108	0.26	3FHL J0521.6+0104 (2.3)
IC190410A	58583.436	310.61 ^{+3.30} _{-3.65}	12.22 ^{+2.84} _{-2.28}	105	0.28	4FGL J2044.0+1036 (1.66)
IC190413A	58586.450	219.33 ^{+0.70} _{-1.32}	11.72 ^{+0.72} _{-0.72}	107	0.29	4FGL J1438.6+1205 (0.49)
IC190413B	58586.665	245.57 ^{+1.23} _{-1.49}	21.98 ^{+1.21} _{-1.44}	115	0.38	... (...)
IC190415A	58588.437	154.86 ^{+2.94} _{-4.70}	5.27 ^{+2.48} _{-1.95}	117	0.30	4FGL J1019.7+0511 (0.11)
IC190422A	58595.250	166.90 ^{+3.21} _{-3.03}	17.39 ^{+2.00} _{-2.56}	170	0.51	4FGL J1112.4+1751 (1.24)
IC190503A	58606.724	120.19 ^{+0.66} _{-0.66}	6.43 ^{+0.68} _{-0.75}	142	0.34	... (...)
IC190504A	58607.768	65.17 ^{+1.67} _{-1.14}	-37.26 ^{+0.61} _{-1.09}	55	0.39	3FHL J0420.4-3744 (0.48)
IC190515A	58618.451	127.88 ^{+0.79} _{-0.83}	12.60 ^{+0.50} _{-0.46}	457	0.82	... (...)
IC190613A	58647.829	312.19 ^{+0.66} _{-0.79}	26.57 ^{+0.75} _{-0.71}	195	0.61	... (...)
IC190619A	58653.552	343.52 ^{+4.13} _{-3.16}	10.28 ^{+2.02} _{-2.76}	199	0.55	SWIFT J2254.2+114 (1.49)
IC190629A	58663.809	29.12 ^{+39.68} _{-118.65}	84.56 ^{+4.66} _{-4.40}	109	0.34	3FHL J0249.7+8434 (1.26)
IC190704A	58668.784	161.81 ^{+2.15} _{-3.91}	26.90 ^{+1.94} _{-1.91}	155	0.49	4FGL J1049.8+2741 (0.97)
IC190712A	58676.052	76.64 ^{+5.23} _{-6.99}	12.75 ^{+4.79} _{-2.82}	109	0.30	4FGL J0502.5+1340 (1.34)
IC190730A	58694.869	226.14 ^{+1.27} _{-1.98}	10.77 ^{+1.03} _{-1.17}	298	0.67	3FHL J1504.3+1030 (0.27)
IC190819A	58714.732	148.54 ^{+2.29} _{-3.30}	1.45 ^{+0.93} _{-0.75}	113	0.29	3FHL J0946.2+0104 (2.01)
IC190922A	58748.405	167.30 ^{+2.81} _{-2.72}	-22.27 ^{+3.39} _{-3.31}	3114	0.20	3FHL J1103.6-2328 (1.77)
IC190922B	58748.961	5.71 ^{+1.19} _{-1.27}	-1.53 ^{+0.90} _{-0.78}	187	0.50	... (...)
IC191001A	58757.840	313.99 ^{+6.94} _{-2.46}	12.79 ^{+1.65} _{-1.64}	218	0.59	4FGL J2052.7+1218 (0.91)
IC191119A	58806.043	229.31 ^{+5.49} _{-4.97}	3.77 ^{+2.47} _{-2.24}	177	0.45	4FGL J1521.1+0421 (1.15)
IC191122A	58809.948	27.03 ^{+1.98} _{-2.72}	0.07 ^{+1.08} _{-1.57}	127	0.33	... (...)

Table 3 continued on next page

Table 3 (continued)

Alert	MJD	RA [°]	Dec [°]	Energy [TeV]	Signalness	Nearest Source (°)
IC191204A	58821.949	80.16 ^{+2.42} _{-1.98}	2.87 ^{+1.05} _{-0.97}	130	0.33	... (...)
IC191215A	58832.465	286.83 ^{+2.27} _{-1.92}	58.45 ^{+2.08} _{-1.86}	133	0.48	... (...)
IC191231A	58848.458	48.47 ^{+5.98} _{-7.65}	20.11 ^{+4.48} _{-3.73}	156	0.46	4FGL J0312.7+2012 (0.28)
IC200109A	58857.987	165.45 ^{+3.60} _{-4.39}	11.80 ^{+1.18} _{-1.29}	375	0.77	3FHL J1103.1+1156 (0.35)
IC200117A	58865.464	116.02 ^{+0.79} _{-1.19}	29.18 ^{+0.86} _{-0.81}	108	0.38	SWIFT J0744.0+29 (0.09)
IC200120A*	58868.784	67.41 ^{+0.40} _{-0.31}	-14.59 ^{+0.23} _{-0.27}	6055	0.31	... (...)
IC200410A	58949.972	242.58 ^{+10.20} _{-10.20}	11.61 ^{+7.83} _{-6.19}	110	0.30	SWIFT J1608.8+12 (0.78)
IC200421A	58960.025	87.93 ^{+3.43} _{-2.81}	8.23 ^{+2.08} _{-1.81}	127	0.33	... (...)
IC200425A	58964.977	99.97 ^{+4.76} _{-3.00}	53.72 ^{+2.25} _{-1.69}	135	0.48	SWIFT J0645.9+53 (1.14)
IC200512A	58981.314	295.18 ^{+1.67} _{-2.24}	15.79 ^{+1.24} _{-1.28}	109	0.32	... (...)
IC200523A	58992.104	338.64 ^{+9.98} _{-6.02}	1.75 ^{+1.79} _{-3.51}	105	0.25	SWIFT J2235.7+01 (0.3)
IC200530A	58999.330	255.37 ^{+2.46} _{-2.55}	26.61 ^{+2.32} _{-3.25}	82	0.59	4FGL J1702.2+2642 (0.2)
IC200614A	59014.529	33.84 ^{+4.79} _{-6.37}	31.61 ^{+2.71} _{-2.25}	115	0.41	4FGL J0220.2+3246 (1.57)
IC200615A	59015.618	142.95 ^{+1.14} _{-1.41}	3.66 ^{+1.16} _{-1.01}	496	0.83	... (...)
IC200620A	59020.127	162.11 ^{+0.62} _{-0.92}	11.95 ^{+0.61} _{-0.46}	114	0.33	... (...)
IC200806A	59067.577	157.25 ^{+1.17} _{-0.87}	47.75 ^{+0.64} _{-0.59}	107	0.40	... (...)
IC200911A	59103.597	51.11 ^{+4.39} _{-10.99}	38.11 ^{+2.31} _{-1.97}	111	0.41	SWIFT J0333.3+37 (1.94)
IC200916A	59108.861	109.78 ^{+1.05} _{-1.41}	14.36 ^{+0.85} _{-0.81}	110	0.32	... (...)
IC200921A	59113.797	195.29 ^{+2.33} _{-1.71}	26.24 ^{+1.46} _{-1.73}	117	0.41	3FHL J1303.0+2435 (1.7)
IC200926A	59118.329	96.46 ^{+0.70} _{-0.53}	-4.33 ^{+0.60} _{-0.75}	670	0.44	... (...)
IC200926B	59118.941	184.75 ^{+3.65} _{-1.54}	32.93 ^{+1.16} _{-0.88}	121	0.43	... (...)
IC200929A	59121.742	29.53 ^{+0.53} _{-0.53}	3.47 ^{+0.71} _{-0.34}	183	0.47	... (...)
IC201007A	59129.918	265.17 ^{+0.48} _{-0.48}	5.34 ^{+0.30} _{-0.19}	683	0.89	... (...)
IC201014A	59136.093	221.22 ^{+0.97} _{-1.19}	14.44 ^{+0.66} _{-0.46}	147	0.41	... (...)
IC201021A	59143.276	260.82 ^{+1.71} _{-1.67}	14.55 ^{+1.31} _{-0.69}	105	0.30	... (...)
IC201114A	59167.629	105.73 ^{+0.92} _{-1.27}	5.87 ^{+1.05} _{-1.01}	214	0.56	... (...)
IC201115A	59168.088	195.12 ^{+1.23} _{-1.45}	1.38 ^{+1.27} _{-1.08}	177	0.46	... (...)
IC201120A	59173.406	307.66 ^{+5.19} _{-5.68}	40.72 ^{+5.02} _{-2.75}	154	0.50	4FGL J2032.6+4053 (0.41)
IC201130A	59183.848	30.54 ^{+1.10} _{-1.27}	-12.10 ^{+1.14} _{-1.11}	203	0.15	4FGL J0206.4-1151 (1.07)
IC201209A	59192.428	6.86 ^{+1.01} _{-1.19}	-9.25 ^{+0.94} _{-1.10}	419	0.19	... (...)
IC201221A	59204.526	261.69 ^{+2.28} _{-2.46}	41.81 ^{+1.25} _{-1.14}	175	0.56	... (...)
IC201222A	59205.039	206.37 ^{+0.88} _{-0.75}	13.44 ^{+0.54} _{-0.34}	186	0.53	... (...)

ACKNOWLEDGEMENTS

The IceCube collaboration acknowledges the significant contributions to this manuscript from Mehr Un Nisa. We also acknowledge support from: USA – U.S. National Science Foundation-Office of Polar Programs, U.S. National Science Foundation-Physics Division, U.S. National Science Foundation-EPSCoR, Wisconsin Alumni Research Foundation, Center for High Throughput Computing (CHTC) at the University of Wisconsin–Madison, Open Science Grid (OSG), Advanced Cyberinfrastructure Coordination Ecosystem: Services & Support (ACCESS), Frontera computing project

at the Texas Advanced Computing Center, U.S. Department of Energy-National Energy Research Scientific Computing Center, Particle astrophysics research computing center at the University of Maryland, Institute for Cyber-Enabled Research at Michigan State University, and Astroparticle physics computational facility at Marquette University; Belgium – Funds for Scientific Research (FRS-FNRS and FWO), FWO Odysseus and Big Science programmes, and Belgian Federal Science Policy Office (Belspo); Germany – Bundesministerium für Bildung und Forschung (BMBF), Deutsche Forschungsgemeinschaft (DFG), Helmholtz Alliance for Astroparticle Physics (HAP), Initiative and Networking Fund of the Helmholtz Association, Deutsches Elektronen Synchrotron (DESY), and High Performance Computing cluster of the RWTH Aachen; Sweden – Swedish Research Council, Swedish Polar Research Secretariat, Swedish National Infrastructure for Computing (SNIC), and Knut and Alice Wallenberg Foundation; European Union – EGI Advanced Computing for research; Australia – Australian Research Council; Canada – Natural Sciences and Engineering Research Council of Canada, Calcul Québec, Compute Ontario, Canada Foundation for Innovation, WestGrid, and Compute Canada; Denmark – Villum Fonden, Carlsberg Foundation, and European Commission; New Zealand – Marsden Fund; Japan – Japan Society for Promotion of Science (JSPS) and Institute for Global Prominent Research (IGPR) of Chiba University; Korea – National Research Foundation of Korea (NRF); Switzerland – Swiss National Science Foundation (SNSF); United Kingdom – Department of Physics, University of Oxford.

APPENDIX

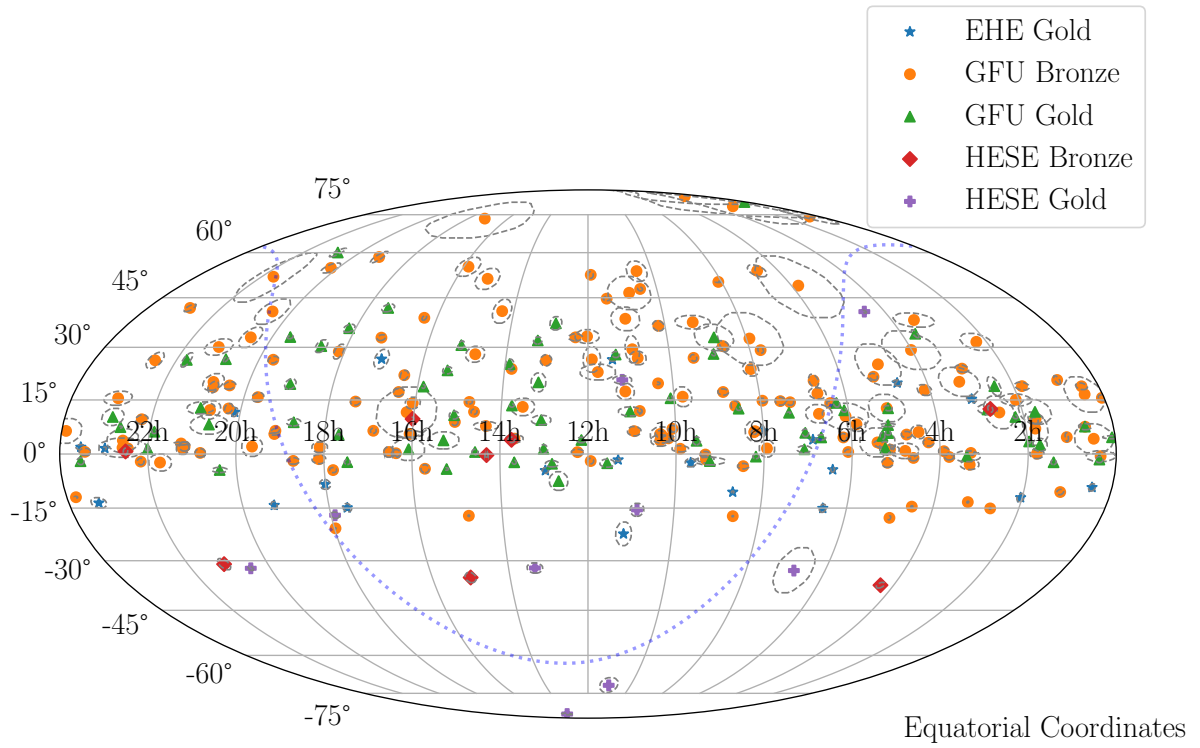


Figure 6. The all-sky distribution of the alerts in the catalog in equatorial coordinates. The blue stars denote EHE, the orange circles GFU Bronze, the green triangles shows GFU Gold, the red diamonds show HESE Bronze, and the purple plus-signs show HESE Gold alerts. The 90% uncertainty contours at the location of each alert are shown by the dashed ellipses.

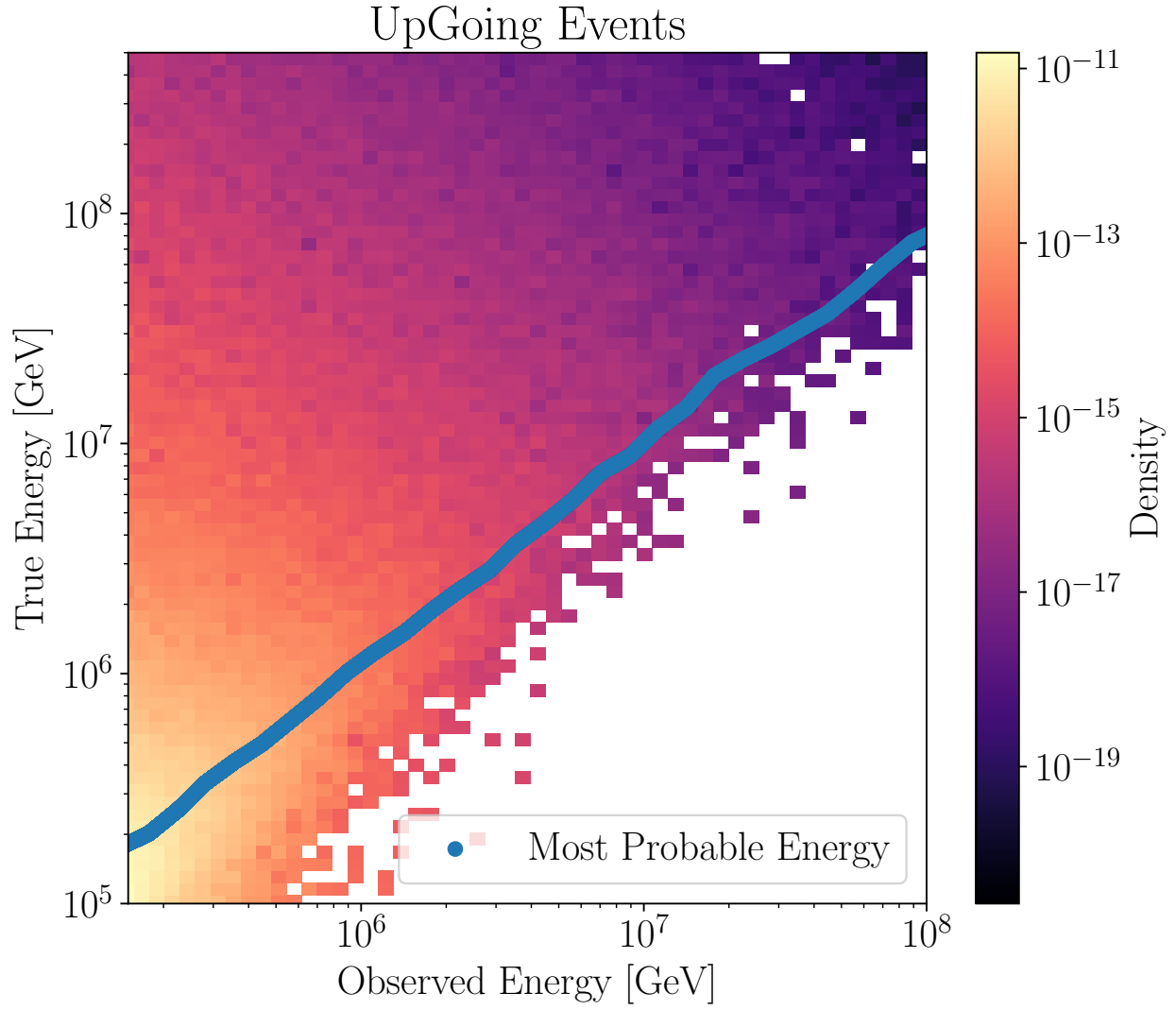


Figure 7. The true neutrino energy as a function of observed energy for simulated up-going GFU Gold events. The most likely estimated neutrino energy is shown in blue.

REFERENCES

- Aartsen, M., Ackermann, M., Adams, J., et al. 2018a, *Science*, 361, 147–151, doi: [10.1126/science.aat2890](https://doi.org/10.1126/science.aat2890)
- . 2018b, *Science*, 361, eaat1378, doi: [10.1126/science.aat1378](https://doi.org/10.1126/science.aat1378)
- Aartsen, M. G., et al. 2013, *Science*, 342, 1242856, doi: [10.1126/science.1242856](https://doi.org/10.1126/science.1242856)
- . 2014a, *JINST*, 9, P03009, doi: [10.1088/1748-0221/9/03/P03009](https://doi.org/10.1088/1748-0221/9/03/P03009)
- . 2014b, *Phys. Rev. Lett.*, 113, 101101, doi: [10.1103/PhysRevLett.113.101101](https://doi.org/10.1103/PhysRevLett.113.101101)
- . 2015, *Eur. Phys. J. C*, 75, 116, doi: [10.1140/epjc/s10052-015-3330-z](https://doi.org/10.1140/epjc/s10052-015-3330-z)
- . 2016a, *JINST*, 11, P11009, doi: [10.1088/1748-0221/11/11/P11009](https://doi.org/10.1088/1748-0221/11/11/P11009)
- . 2016b, *Astrophys. J.*, 833, 3, doi: [10.3847/0004-637X/833/1/3](https://doi.org/10.3847/0004-637X/833/1/3)
- . 2017a, *JINST*, 12, P03012, doi: [10.1088/1748-0221/12/03/P03012](https://doi.org/10.1088/1748-0221/12/03/P03012)
- . 2017b, *Astropart. Phys.*, 92, 30, doi: [10.1016/j.astropartphys.2017.05.002](https://doi.org/10.1016/j.astropartphys.2017.05.002)
- . 2017c, *Astrophys. J.*, 835, 151, doi: [10.3847/1538-4357/835/2/151](https://doi.org/10.3847/1538-4357/835/2/151)
- Aartsen, M. G., et al. 2019, *ApJ*, 886, 12, doi: [10.3847/1538-4357/ab4ae2](https://doi.org/10.3847/1538-4357/ab4ae2)
- Aartsen, M. G., et al. 2020a, *Phys. Rev. Lett.*, 125, 121104, doi: [10.1103/PhysRevLett.125.121104](https://doi.org/10.1103/PhysRevLett.125.121104)
- . 2020b, *Phys. Rev. Lett.*, 124, 051103, doi: [10.1103/PhysRevLett.124.051103](https://doi.org/10.1103/PhysRevLett.124.051103)
- . 2021, *Nature*, 591, 220, doi: [10.1038/s41586-021-03256-1](https://doi.org/10.1038/s41586-021-03256-1)
- Abbasi, R., Ackermann, M., Adams, J., et al. 2009, *Nuclear Instruments and Methods in Physics Research Section A: Accelerators, Spectrometers, Detectors and Associated Equipment*, 601, 294–316, doi: [10.1016/j.nima.2009.01.001](https://doi.org/10.1016/j.nima.2009.01.001)
- Abbasi, R., et al. 2011, *Phys. Rev. D*, 83, 012001, doi: [10.1103/PhysRevD.83.012001](https://doi.org/10.1103/PhysRevD.83.012001)
- . 2012, *Astropart. Phys.*, 35, 615, doi: [10.1016/j.astropartphys.2012.01.004](https://doi.org/10.1016/j.astropartphys.2012.01.004)
- . 2013, *Nuclear Instruments and Methods in Physics Research Section A: Accelerators, Spectrometers, Detectors and Associated Equipment*, 700, 188, doi: [10.1016/j.nima.2012.10.067](https://doi.org/10.1016/j.nima.2012.10.067)
- Abbasi, R., Abdou, Y., Ackermann, M., et al. 2013, *Nuclear Instruments and Methods in Physics Research A*, 703, 190, doi: [10.1016/j.nima.2012.11.081](https://doi.org/10.1016/j.nima.2012.11.081)
- Abbasi, R., et al. 2021a, *Phys. Rev. D*, 104, 022002, doi: [10.1103/PhysRevD.104.022002](https://doi.org/10.1103/PhysRevD.104.022002)
- . 2021b, *JINST*, 16, P07041, doi: [10.1088/1748-0221/16/07/P07041](https://doi.org/10.1088/1748-0221/16/07/P07041)
- . 2021c, *PoS, ICRC2021*, 1045, doi: [10.22323/1.395.1045](https://doi.org/10.22323/1.395.1045)
- . 2021d, *Astrophys. J.*, 910, 4, doi: [10.3847/1538-4357/abe123](https://doi.org/10.3847/1538-4357/abe123)
- . 2022a, *Astrophys. J.*, 928, 50, doi: [10.3847/1538-4357/ac4d29](https://doi.org/10.3847/1538-4357/ac4d29)
- . 2022b, *The Cryosphere Discussions*, 2022, 1, doi: [10.5194/tc-2022-174](https://doi.org/10.5194/tc-2022-174)
- . 2022c, *Astrophys. J.*, 926, 59, doi: [10.3847/1538-4357/ac3cb6](https://doi.org/10.3847/1538-4357/ac3cb6)
- . 2022d, arXiv Pre-print, <https://arxiv.org/abs/2210.04930>
- . 2023, arXiv preprint, doi: [10.48550/arXiv.2304.12675](https://doi.org/10.48550/arXiv.2304.12675)
- Abbott, B. P., et al. 2017, *Astrophys. J. Lett.*, 848, L12, doi: [10.3847/2041-8213/aa91c9](https://doi.org/10.3847/2041-8213/aa91c9)
- Abdollahi, S., et al. 2020, *Astrophys. J. Suppl.*, 247, 33, doi: [10.3847/1538-4365/ab6bcb](https://doi.org/10.3847/1538-4365/ab6bcb)
- Ajello, M., et al. 2017, *Astrophys. J. Suppl.*, 232, 18, doi: [10.3847/1538-4365/aa8221](https://doi.org/10.3847/1538-4365/aa8221)
- Albert, A., et al. 2020, *Astrophys. J.*, 905, 76, doi: [10.3847/1538-4357/abc2d8](https://doi.org/10.3847/1538-4357/abc2d8)
- Amin, N. M. B. 2021, *Journal of Physics: Conference Series*, 2156, 012217, doi: [10.1088/1742-6596/2156/1/012217](https://doi.org/10.1088/1742-6596/2156/1/012217)
- Ayala Solares, H. A., et al. 2020, *Astropart. Phys.*, 114, 68, doi: [10.1016/j.astropartphys.2019.06.007](https://doi.org/10.1016/j.astropartphys.2019.06.007)
- Blaufuss, E., Kintscher, T., Lu, L., & Tung, C. F. 2020, *PoS, ICRC2019*, 1021, doi: [10.22323/1.358.1021](https://doi.org/10.22323/1.358.1021)
- Dzhappuev, D. D., et al. 2020, *JETP Lett.*, 112, 753, doi: [10.1134/S0021364020240029](https://doi.org/10.1134/S0021364020240029)
- Górski, K. M., Hivon, E., Banday, A. J., et al. 2005, *Astrophys. J.*, 622, 759, doi: [10.1086/427976](https://doi.org/10.1086/427976)
- Haack, C., & Wiebusch, C. 2017, in *Proceedings of 35th International Cosmic Ray Conference — PoS(ICRC2017)*, Vol. 301, 1005, doi: [10.22323/1.301.1005](https://doi.org/10.22323/1.301.1005)
- Heck, D., Knapp, J., Capdevielle, J. N., Schatz, G., & Thouw, T. 1998
- Kankare, E., Huber, M., Smartt, S. J., et al. 2019, *A&A*, 626, A117, doi: [10.1051/0004-6361/201935171](https://doi.org/10.1051/0004-6361/201935171)
- Kronmueller, M., & Glauch, T. 2019, in *International Cosmic Ray Conference*, Vol. 36, 36th International Cosmic Ray Conference (ICRC2019), 937, doi: [10.22323/1.358.0937](https://doi.org/10.22323/1.358.0937)
- Necker, J., de Jaeger, T., Stein, R., et al. 2022, *Monthly Notices of the Royal Astronomical Society*, 516, 2455, doi: [10.1093/mnras/stac2261](https://doi.org/10.1093/mnras/stac2261)
- Oh, K., et al. 2018, *ApJS*, 235, 4, doi: [10.3847/1538-4365/aaa7fd](https://doi.org/10.3847/1538-4365/aaa7fd)
- Pence, W. D., Chiappetti, L., Page, C. G., Shaw, R. A., & Stobie, E. 2010, *A&A*, 524, A42, doi: [10.1051/0004-6361/201015362](https://doi.org/10.1051/0004-6361/201015362)

Plavin, A., Kovalev, Y. Y., Kovalev, Y. A., & Troitsky, S. 2020, *Astrophys. J.*, 894, 101,
doi: [10.3847/1538-4357/ab86bd](https://doi.org/10.3847/1538-4357/ab86bd)

Schönert, S., Gaisser, T. K., Resconi, E., & Schulz, O. 2009, *Phys. Rev. D*, 79, 043009,
doi: [10.1103/PhysRevD.79.043009](https://doi.org/10.1103/PhysRevD.79.043009)

Stein, R., et al. 2021, *Nature Astron.*, 5, 510,
doi: [10.1038/s41550-020-01295-8](https://doi.org/10.1038/s41550-020-01295-8)

Wakely, S. P., & Horan, D. 2008, in *International Cosmic Ray Conference*, Vol. 3, *International Cosmic Ray Conference*, 1341–1344